

**The role of physicochemical parameters on  
polybutylcyanoacrylate nanoparticles' delivery to the  
central nervous system**

Thesis

for the degree of

**doctor rerum naturalum (Dr. rer. nat.)**

approved by the Faculty of Natural Sciences of Otto von Guericke University Magdeburg

by BSc, MMed Qing YOU

born on 16.08.1986 in Henan

Examiner: Prof. Dr. Bernhard A. Sabel

Prof. Dr. Hans-Joachim Galla

submitted on: 27.08.2019

defended on: 03.02.2020

## ABSTRACT

Because the blood-brain barrier (BBB) is an obstacle for drug-delivery, carrier systems such as polybutylcyanoacrylate (PBCA) nanoparticles (NPs) have been studied. Yet, little is known of how the physicochemical features such as size and surface charge influence the BBB passage *in vivo*. Firstly I used a rat model of *in vivo* imaging of the retina - which is brain tissue and can reflect the situation at the BBB - to study how size and surface charge determine NPs' delivery kinetics across the blood-retina barrier (BRB). I also analyzed the co-incubation of NPs with serum *in vitro* to understand the interactions of NPs with blood. Then I investigated the physicochemical mechanisms underlying these different behaviors of NPs at biological barriers and their influence on the cellular distribution. Retinal whole-mounts from rats injected *in vivo* with fluorescent NPs were processed for retina imaging *ex vivo* to obtain a detailed distribution of NPs with cellular resolution in retinal tissue. In addition, I analyzed the NPs' body distribution *in vivo* to explore the systematic interactions. The key results are as follows:

- Minor changes in composition of poloxamer 188-modified, DEAE-dextran-stabilized (PDD) PBCA NPs, although only slightly altering the physicochemical parameters, such as size or surface charge, substantially influence NPs' delivery kinetics across the BRB *in vivo*. Decreasing the Z-average size from 272 nm to 172 nm by centrifugation reduced the BRB passage of the NPs substantially. Varying the zeta-potential within the narrow range of 0-15 mV by adding different amounts of stabilizer revealed that 0 mV and 15 mV were less desirable than 5 mV which facilitated the BRB passage.
- NPs with medium charge and small size were relatively stable in blood, while other NP variations rapidly agglomerated or degraded.
- In line with the *in vivo* imaging results, NPs with larger size and medium surface

charge accumulated more readily in brain tissue and they could be more easily detected in retinal ganglion cells (RGCs), demonstrating the suitability of these NPs for drug delivery into neurons.

- Other NP variations accumulated more in peripheral organs which may reduce the passage of these particles into brain tissue via a “steal effect”-mechanism.

Thus, systemic interactions significantly determine the potential of NPs to deliver markers or drugs to the central nervous system (CNS). In this way, minor changes of NPs’ physicochemical parameters can significantly impact alterations in their rate of brain/body biodistribution.

## ZUSAMMENFASSUNG

Da die Blut-Hirn-Schranke (BHS) ein Hindernis für die Arzneimittelwirksamkeit darstellt, wurden Trägersysteme wie Polybutylcyanoacrylat (PBCA)-Nanopartikel (NP) untersucht. Es ist jedoch wenig bekannt, wie die physiochemischen Merkmale wie Größe und Oberflächenladung die BHS-Passage *in vivo* beeinflussen. Zunächst verwendete ich ein Rattenmodell der *In-vivo*-Bildgebung der Netzhaut, die Gehirngewebe ist und die Situation an der BHS widerspiegeln kann, und Größe und Oberflächenladung die Abgabekinetik von NP über die Blut-Netzhaut-Schranke (BNS) zu bestimmen. Ich analysierte auch die Co-Inkubation von NP mit Serum *in vitro*, um die Wechselwirkungen von NP mit Blut zu verstehen. Ausschließend untersuchte ich die physikochemischen Mechanismen, die diesen unterschiedlichen Verhaltensweisen von NP an biologischen Barrieren zugrunde liegen sowie ihren Einfluss auf die Zellverteilung. Retinale Ganzpräparate von Ratten, denen *in vivo* fluoreszierende-NP injiziert worden waren, wurden zur Bildgebung der Retina *ex vivo* verarbeitet, um eine detaillierte Verteilung der NP mit zellulärer Auflösung in Netzhautgewebe zu bestimmen. Zusätzlich analysierte ich die Körperverteilung der NP *in vivo*, um die systematischen Wechselwirkungen zu untersuchen. Die wichtigsten Ergebnisse lauten wie folgt:

- Geringe Änderungen in der Zusammensetzung von Poloxamer 188-modifizierten, DEAE-Dextran-stabilisierten PBCA-NP beeinflussen die Abgabekinetik von NP über den BNS *in vivo*, obwohl sie die physikalisch-chemischen Parameter wie Größe oder Oberflächenladung nur geringfügig ändern. Das Verringern der Z-Durchschnittsgröße von 272 nm auf 172 nm durch Zentrifugation verringerte den BNS-Durchgang der NP erheblich. Das Variieren des Zeta-Potentials innerhalb des engen Bereichs von 0 bis 15 mV durch Zugabe verschiedener Mengen an Stabilisator zeigte, dass 0 mV und 15 mV weniger wünschenswert waren als 5 mV, was den BNS-Durchgang erleichterte.

- NP mit mittlerer Ladung und kleiner Größe waren im Blut relativ stabil, während andere NP-Variationen schnell agglomerierten oder abgebaut wurden.
- Entsprechend den Ergebnissen der *In-vivo*-Bildgebung reichert sich NP mit größerer Größe und mittlerer Oberflächenladung leichter im Gehirngewebe an und konnten in retinalen Ganglienzellen leichter nachgewiesen werden, was für die Eignung dieser NP für die Wirkstoffabgabe in Neuronen spricht.
- Andere NP-Variationen reichern sich in peripheren Organen stärker an, was den Durchgang dieser Partikel in das Gehirngewebe über einen "Steal-Effekt"-Mechanismus verringern kann.

Somit haben systemische Wechselwirkungen einen signifikant Einfluss auf das Potenzial von NP, Marker oder Arzneimittel an das Zentralnervensystem abzugeben. Auf diese Weise können geringfügige Änderungen der physikochemischen Parameter von NP erhebliche Auswirkungen auf Änderungen ihrer Geschwindigkeit der biologischen Verteilung von Gehirn und Körper haben.

# TABLE OF CONTENTS

<b>Abstract.....</b>	<b>I</b>
<b>Zusammenfassung.....</b>	<b>III</b>
<b>Abbreviations .....</b>	<b>9</b>
<b>List of Figures and Tables .....</b>	<b>10</b>
1 General Introduction .....	1
1.1 A major problem in neuropharmacology .....	1
1.2 Blood-brain barrier .....	1
1.2.1 What is the blood-brain barrier?.....	1
1.2.2 Mechanisms of the passage .....	3
1.2.3 Models to study the passage.....	3
1.2.4 A surrogate model - blood-retina barrier.....	4
1.3 Drug carriers to pass blood-brain barrier .....	5
1.3.1 Drug carriers.....	5
1.3.2 What is needed for a perfect carrier? .....	5
1.3.3 Mechanisms of the passage for nanoparticles .....	6
1.4 Physicochemical parameters of nanoparticles and their role .....	7
1.4.1 Surface.....	7
1.4.2 Size .....	8
1.4.3 Charge .....	8

1.5	Poly butylcyanoacrylate nanoparticles .....	9
1.5.1	Choice of nanoparticle .....	9
1.5.2	Polymerization .....	9
1.5.3	Surface modification .....	11
1.6	Aims of the dissertation.....	11
2	Major effects on BRB passage kinetic by minor alterations in design .....	14
2.1	Introduction .....	14
2.2	Materials and Methods .....	17
2.2.1	Equipments.....	17
2.2.2	Reagents .....	17
2.2.3	Nanoparticle production.....	18
2.2.4	Nanoparticle characterizations .....	20
2.2.5	Animals .....	20
2.2.6	Co-incubation of nanoparticles and serum.....	21
2.2.7	Nanoparticle injection .....	22
2.2.8	<i>In vivo</i> retina imaging and kinetic studies.....	22
2.2.9	Image analysis .....	23
2.2.10	Statistical analysis.....	23
2.3	Results .....	25
2.3.1	Nanoparticle characterizations .....	25
2.3.2	Degradation and agglomeration in blood.....	25

2.3.3	No unspecific BRB opening.....	30
2.3.4	Adsorbed labeling versus incorporated labeling .....	30
2.3.5	BRB passage kinetic.....	31
2.3.6	Effects of surface charge .....	32
2.3.7	Effects of size .....	33
2.4	Discussion .....	35
3	Physicochemical parameters affect distribution in CNS via systematic interactions.....	40
3.1	Introduction .....	40
3.2	Materials and Methods .....	43
3.2.1	Equipments.....	43
3.2.2	Reagents .....	43
3.2.3	Animals .....	44
3.2.4	RGC labeling.....	45
3.2.5	Nanoparticle production.....	45
3.2.6	Nanoparticle characterization.....	46
3.2.7	Nanoparticle injection .....	46
3.2.8	<i>Ex vivo</i> retina imaging and biodistribution studies .....	46
3.2.9	Biodistribution in brain and peripheral organs.....	47
3.2.10	Statistical analysis.....	49
3.3	Results .....	50



3.3.1	Nanoparticle characterizations .....	50
3.3.2	Biodistribution in retina cells .....	52
3.3.3	Biodistribution in the brain and peripheral organs .....	56
3.4	Discussion .....	58
4	General discussion .....	62
4.1	Design of the Studies.....	62
4.2	Protein corona-first interaction with blood .....	63
4.3	Degradation and agglomeration in blood.....	63
4.4	Clearance by the MPS .....	64
4.5	Effects on circulation time .....	65
4.6	Possible mechanisms of passage .....	66
4.7	General conclusions .....	67
5	References.....	69
	<b>Ehrenerklärung.....</b>	<b>79</b>

## **ABBREVIATIONS**

BBB	blood-brain barrier
BRB	blood-retina barrier
CD	carbon dots
CNS	central nervous system
CSF	cerebrospinal fluid
Da	Dalton
FI	fluorescence intensity
MGV	mean grey value
MPS	mononuclear phagocyte system
NP	nanoparticle
PBCA	polybutylcyanoacrylate
PDD	poloxamer 188-modified, DEAE-dextran-stabilized
PDI	polydispersity index
PEG	Polyethylene glycol
RGC	retinal ganglion cell
ROI	region of interest
SEM	scanning electron microscope

## LIST OF FIGURES AND TABLES

### Figures

Figure 1. The structure illustration of the BBB.....	2
Figure 2. BBB vs. BRB.....	4
Figure 3. The NPs developed in the past decade assisting drugs across the BBB.....	5
Figure 4. Flowchart of the BBB penetration mechanisms of NPs.....	7
Figure 5. Chemical structure of PBCA.....	10
Figure 6. Polymerization mechanisms of PBCA.....	10
Figure 7. NPs with different surfactants.....	12
Figure 8. NP production and minor alterations in design.....	19
Figure 9. <i>In vivo</i> imaging of retina.....	22
Figure 10. Representative particle size distribution of NPs at the start and end of 10 min co-incubation.....	27
Figure 11. Morphology of NPs with or without co-incubation.....	28
Figure 12. “BRB opening” test.....	30
Figure 13. Adsorbed labeling vs. incorporated labeling.....	31
Figure 14. Representative images to demonstrate the NPs’ kinetic of BRB passage..	32
Figure 15. Kinetic profile of NPs with different surface charges.....	33
Figure 16. Kinetic profile of NPs with different sizes.....	34
Figure 17. Retrograde labeling of RGCs by injecting a fluorescent dye into the superior colliculus.....	45

Figure 18. <i>Ex vivo</i> imaging of retina.....	47
Figure 19. Stability of PDD PBCA NPs.....	51
Figure 20. Release rate of Rhodamine 123.....	51
Figure 21. Bound rate of Rhodamine 123.....	52
Figure 22. Percentage of RGCs with accumulated PDD PBCA NPs over total amount of RGCs.....	53
Figure 23. Representative <i>ex vivo</i> imaging of fluorescence signals in the retina tissue under 5 × magnification 30 min after <i>i.v.</i> administration of PDD PBCA NPs.....	54
Figure 24. Representative <i>ex vivo</i> imaging of fluorescence signals in the retina tissue under 50 × magnification 30 min after <i>i.v.</i> administration of PDD PBCA NPs.....	55
Figure 25. Biodistribution of PDD PBCA NPs with different surface charges in brain and other main organs of rats 30 min after <i>i.v.</i> administration.....	57
Figure 26. Biodistribution of medium-charge PDD PBCA NPs with different sizes in brain and other main organs of rats 30 min after <i>i.v.</i> administration.....	57

## **Tables**

Table 1. Compositions of PDD PBCA NPs.....	20
Table 2. Characterizations of PDD PBCA NPs.....	25
Table 3. Z-average size and PDI of NPs at the start and the end of the 10 min co-incubation with serum.....	27
Table 4. Preparations of standard series.....	48
Table 5. Linear regression equations of concentrations of Rhodamine 123 in blood or organ homogenates.....	48
Table 6. Characterizations of PDD PBCA NPs .....	50

# 1 General Introduction

## 1.1 A major problem in neuropharmacology

Although there is a great need for new drug treatments for various brain diseases (*i.e.*, Stroke, Alzheimer, traumatic brain injury, visual system disorders, etc.), drug development is severely hampered by the fact that 98% of potentially effective substances fail to reach the brain tissue because they cannot cross the blood-brain barrier (BBB).

## 1.2 Blood-brain barrier

### 1.2.1 What is the blood-brain barrier?

The endothelial cells that make up the blood vessel walls separate the circulating blood from parenchyma, extracellular matrix and extracellular fluid. In the CNS, together with pericytes, glia endfeet and basal lamina, the endothelial cells are connected by tight junctions to form a highly selective membrane which comprises the BBB (Figure 1; Mayer F, *et al.*, 2009). It shields the brain tissue from unwanted molecules through different mechanisms that regulate the exchange of molecules, ions and even NPs cross this barrier, including active transport based systems and diffusion based systems (Zhou Y, *et al.*, 2018). In this way the BBB is a “gate keeper” for metals, hormones, toxicants and neurotransmitters, thus ensuring a stable homeostasis which is critical as the neurons react quite sensitively to any changes in the extracellular milieu (Luissint AC, *et al.*, 2012). The downside of this tight control by the BBB is that it comprises a problem for most drugs as it prevents their passage into the brain. The BBB prevents the entry of over 95% of small molecules and almost 100% of large molecules (Pardridge WM, 2007).

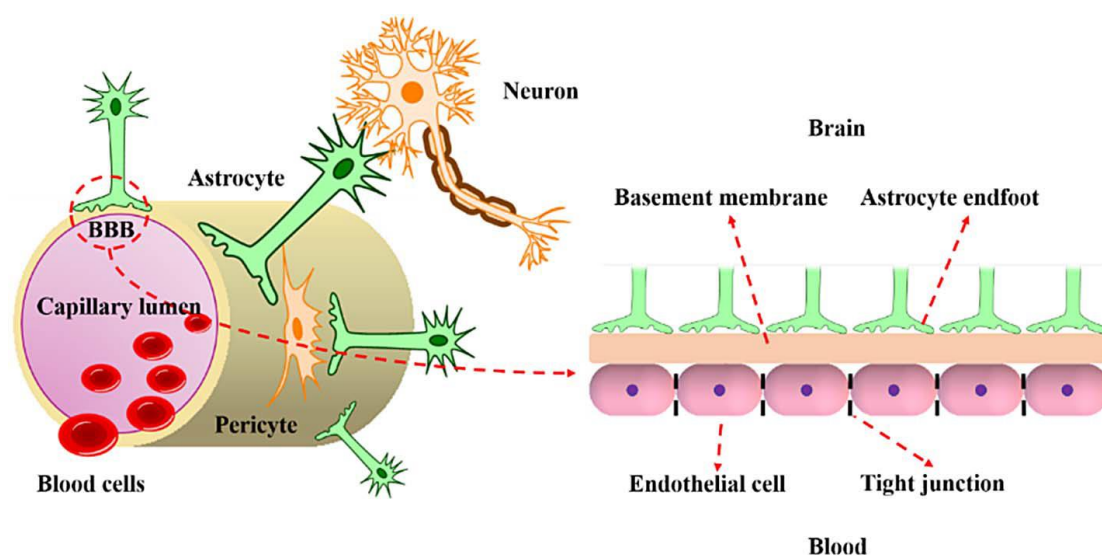


**Figure 1.** The structure illustration of the BBB ( from Zhou Y, *et al.*, 2018).

The discovery of the BBB can be traced back to 1885 when a German bacteriologist stained animal organs by injecting a water-soluble aniline dye into the peripheral circulation which failed to stain the brain and the cerebrospinal fluid (CSF) (Béduneau A, *et al.*, 2007). The widely accepted explanation then was related to the selective binding affinities of different organs. However, the same phenomenon was observed in another experiment in 1913 by injecting Trypan blue, a water-soluble azo dye, into the CSF of dogs (Goldmann EE, 1912). Only the CNS including brain and the spinal cord got stained. In the same year, the name “BBB” was first put forward by Edwin Goldman based on his observation and hypothesis. The hypothesis stated that there must exist a barrier preventing the transfer of dyes between blood and brain, which was previously proposed by Bield, Kraus, and Lewandowsky (Ribatti D, *et al.*, 2006). However, the actual membrane barrier was not observed until the scanning electron microscopy (SEM) was invented in 1937 and later widely introduced into the medical research field.

### **1.2.2 Mechanisms of the passage**

The mechanism of passive diffusion of the molecule across the BBB is dependent on its structural and physicochemical properties, such as molecular size, charge, hydrogen bonding potential, and lipophilicity (Pauletti GM, *et al.*, 1997). Besides compounds essential for brain homeostasis, such as amino acids, hexoses, neuropeptides, and proteins which are transported into the brain via specific carriers, only small lipophilic molecules of less than 500 Dalton (Da) are able to cross this complex barrier (Wu D, *et al.*, 1998; Pardridge WM, *et al.*, 1998). Moreover, even after successful endothelial cell absorption, active efflux mechanisms (ATP-binding cassette transporter) may pump these molecules back into the blood stream (Begley DJ, *et al.*, 1996). Especially the P-glycoprotein expressed in the luminal membrane of the BBB endothelium limits the brain access of a wide range of systemically administered drugs (Cordon-Cardo C, *et al.*, 1989).

### **1.2.3 Models to study the passage**

The standard method for analysing pharmacokinetic parameters of the BBB passage is the *in vivo* method of the “brain/plasma ratio” (Reichel A, 2006). Other techniques are “in situ brain perfusion”, “brain uptake index” or microdialysis (Elmqvist WF, *et al.*, 1997; Dagenais C, *et al.*, 2005). However, these techniques are rather complex, laborious and costly which limits their use for drug testing. In addition, the cranial window is a newly developed model to study the BBB for long-term imaging. But no matter how skillful an experimenter is, a cranial window is always a traumatic procedure and therefore conditions of the brain tissue may not be as naive as with the surrogate model I have used.

### 1.2.4 A surrogate model - blood-retina barrier

The retina is the only brain tissue available for non-invasive *in vivo* microscopic imaging. The BRB is more permeable than the BBB for some compounds (Toda, *et al.*, 2011) and the trans-endothelial electrical resistance of the BRB *in vitro* reported by Campbell M *et al.* is around  $50 \Omega/\text{cm}^2$  (Campbell M, *et al.*, 2011), which is lower than BBB *in vitro* over  $200 \Omega/\text{cm}^2$  (Freese C, *et al.*, 2017). Yet, the BRB and BBB are similar regarding the expression of efflux proteins and the permeability for many drugs (Steuer H, *et al.*, 2004 and 2005). Regarding passage of NPs into brain tissue, the preliminary data suggest that the results from our BRB model are also valid for the situation at the BBB (Figure 2). I therefore used the eye as a “window to the brain”. With this model I visualized the function of the inner BRB which is being formed of the tight junctions between the retinal capillary endothelial cells (Cunha-Vaz J, *et al.*, 2011).

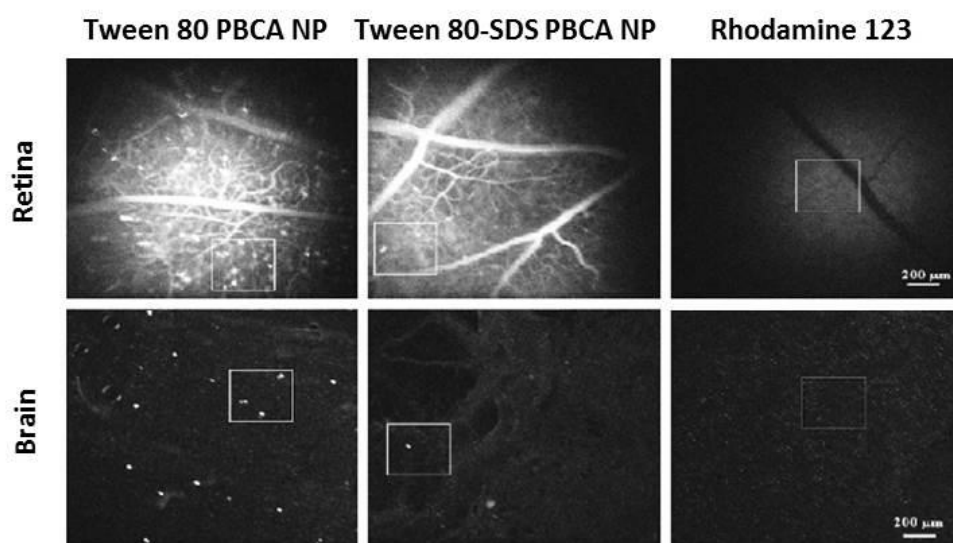


**Figure 2.** BBB vs. BRB. We tested whether the results from our BRB model are also valid for the situation at the BBB by comparing *in vivo* retina and *ex vivo* brain slice images after injection of fluorescent NPs. The High-permeable Tween 80 PBCA NPs, low-permeable Tween 80-SDS PBCA NPs and Rhodamine 123 (fluorescent marker without NP as control group) showed comparable fluorescence signals between retina and brain tissue.



## 1.3 Drug carriers to pass blood-brain barrier

### 1.3.1 Drug carriers

Because the tight control of the BBB poses a problem for pharmacotherapies of CNS diseases, many potential drug carriers have been explored to overcome this limitation. The fundamental approach was to mask the unfavorable physicochemical characteristics of the incorporated drugs and transport them across the BBB. Different NP designs and materials were developed for different tasks (Figure 3). The most common drug carriers are micelles, liposomes and polymeric nanoparticles (Frenkel V, 2008; Hernot S & Klibanov AL, 2008; Jokerst JV, *et al.*, 2011).

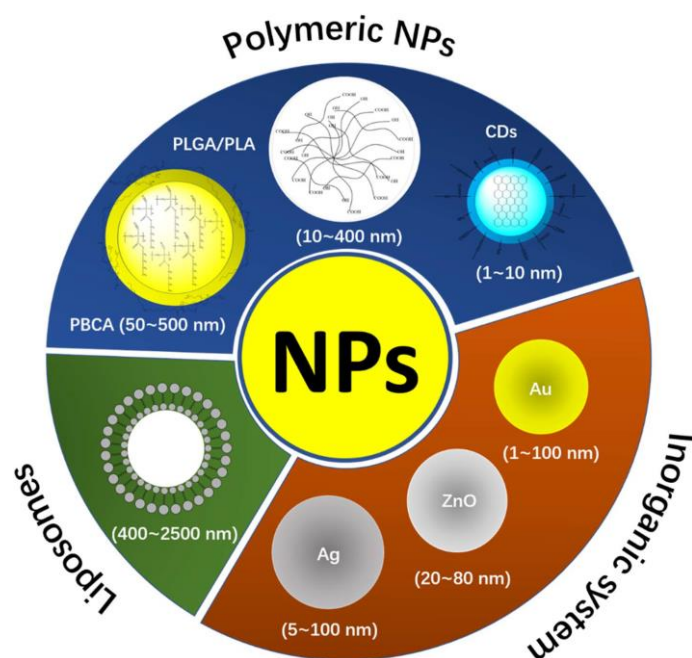


**Figure 3.** The NPs developed in the past decade assisting drugs across the BBB (from Zhou Y, *et al.*, 2018)

### 1.3.2 What is needed for a perfect carrier?

Certain criteria are common for all drug carriers and must be met in order to be

accepted as a drug carrier. First of all, the drug carrier must be biocompatible, which means no negative reactions when placed in the body. Ideally, it should travel unnoticed through the body. It needs to be biodegradable, or at least excretable by the kidneys to avoid accumulation in the body, which again can lead to a toxic reaction. The circulation time of the drug carrier must be sufficiently long in order to bring the drug carrier load to its right destination. Finally, the “ideal” drug carrier should somehow be selective, so it accumulates only in the diseased regions, and leave healthy cells unharmed behind. The concentration of the NPs in target region should be high enough to achieve an effective treatment. The design of the NP is often quite complex in order to fulfill all these criterias.

### **1.3.3 Mechanisms of the passage for nanoparticles**

The BBB penetration mechanism can be divided into active and passive transport routes (Figure 4; Zhou Y, *et al.*, 2018). The passive transport routes indicate energy-independent processes, for instance, simple diffusion. And the passive diffusion of drugs usually occurs in tumor cells via the enhanced permeability and retention effect (Maeda H, *et al.*, 2000). In contrast, the active transport routes include receptor- and adsorption- mediated endocytosis and carrier-mediated transport, which all require the hydrolysis of adenosine triphosphate (Hervé F, *et al.*, 2008; Pulicherla KK, *et al.*, 2015; Grabrucker AM, *et al.*, 2016). Also, for instance, the small and stereospecific pores in the carrier-mediated transport system restrict the transport of large-molecular drugs (Jounes AR *et al.*, 2007). Instead, most carbon dots (CDs) have an ultra-small size (1–10 nm) and versatile surface functionalities (Bhunias SK, *et al.*, 2013), which would be in favor of the delivery of large drug molecules via the carrier-mediated transport by covalently conjugating with drugs (Pardridge WM, 2005).

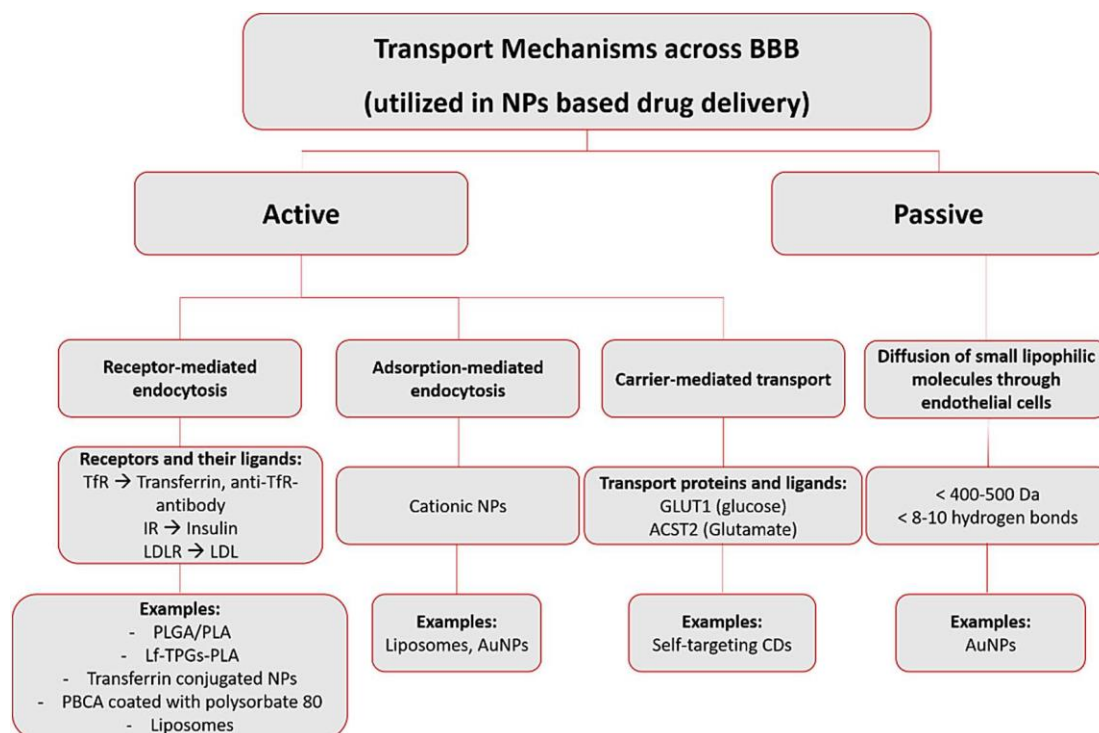


**Figure 4.** Flowchart of the BBB penetration mechanisms of NPs (from Zhou Y, *et al.*, 2018). TfR, transferrin receptor; IR, insulin receptor; LDL, low-density lipoprotein; LDLR, low-density lipoprotein receptor; Lf, lactoferrin; TPGS, D- $\alpha$ -tocopheryl polyethylene glycol 1000 succinate. Small lipophilic molecules (< 400 Da) diffuses passively through endothelial cells. The penetration of charged molecules such as cationic NPs depends on adsorption-mediated endocytosis while the delivery of large molecules with high hydrophilicity such as transferrin requires active transport route (*i.e.*, receptor-mediated endocytosis).

## 1.4 Physicochemical parameters of nanoparticles and their role

### 1.4.1 Surface

One popular way to optimize the BBB passage of the NPs is to modify their surface as, for example, to allow receptor-mediated endocytosis in brain capillary endothelial cells (Gabathuler R, *et al.*, 2010; Wohlfart S, *et al.*, 2012; Zhou Y, *et al.*, 2018).

Modifications of NPs' surface with covalently attached targeting ligands like apolipoprotein A-ligand (Kreuter J, *et al.*, 2007; Petri B, *et al.*, 2007) or coating NPs with surfactants like polysorbate 80 – which attracts a corona of plasma proteins - induce such receptor-mediated uptake (Wohlfart S, *et al.*, 2012). For polysorbate 80-coated PBCA NPs, several mechanisms have been confirmed: (1) endocytotic uptake of endothelial cells; (2) inhibition of the P-glycoprotein; (3) disruption of the BBB. Despite these achievements, the *in vivo* efficacies of most NP modifications are still quite limited (Wang CX, *et al.*, 2009).

### 1.4.2 Size

In many studies, small size was found to be beneficial for BBB passage of NPs (Wohlfart S, *et al.*, 2012; Zhou Y, *et al.*, 2018). It has also been suggested that the size limitation for movement of NPs, *i.e.*, by diffusion, in the extracellular space is 64 nm maximum (Thorne RG, *et al.*, 2006). For Tween 80 coated NPs, the recommended size for the BBB passage is below 100 nm (Gao K, *et al.*, 2006). In contrast our previous experiments demonstrated that the smallest PBCA NP modified with poloxamer 188-SDS (Z-average size 87 nm) was not effective to pass the BRB, whereas the very large NP modified with DEAE-dextran-poloxamer 188 (464 nm) passed the BRB efficiently as well as the middle-sized NPs modified with Tween 80 (143 nm) (Voigt N, *et al.*, 2014).

### 1.4.3 Charge

With reference to surface charge, negative charge has regularly been demonstrated to be beneficial for BBB passage of NPs (Zhou Y, *et al.*, 2018), but higher internalization rates are associated with positively-charged NPs because of the negatively-charged cell membrane composition (Wohlfart S, *et al.*, 2012). Regarding the passage into

brain tissue, however, our previous *in vivo* experiments showed that the positively-charged PBCA NP modified with Tween 80-dextran (zeta-potential 5 mV) and DEAE-dextran (20 mV) passed the BRB efficiently as well as the NP modified with Tween 80 (-26 mV) and poloxamer 188-dextran (-16 mV) (Voigt N, *et al.*, 2014). We hypothesized that the physicochemical parameters can influence NP's BBB passage not only by single up-take mechanisms but also by multiple *in vivo* ways.

## **1.5 Poly butylcyanoacrylate nanoparticles**

### **1.5.1 Choice of nanoparticle**

The biocompatible and biodegradable polymeric NPs such as PBCA NPs have been investigated intensively since 1995 (Kreuter J, *et al.*, 1995; Alyautdin RN, *et al.*, 1998; Olivier JC, *et al.*, 1999). Cyanoacrylates have been widely used in drug delivery because of their favorable properties such as stability, biodegradability, biocompatibility and targetability (Gelperina SE *et al.*, 2002; Pereverzeva E *et al.*, 2007 and 2008). I chose PBCA NPs as promising polymeric drug carriers, as they have a well-characterized, good safety profile and have already been used in patient studies (Zhou Q, *et al.*, 2009).

### **1.5.2 Polymerization**

I synthesized PBCA NPs by a mini-emulsion process. Figure 5 & 6 shows the chemical structure and polymerization mechanisms of PBCA. The most important advantage of preparation of nanocarriers using the miniemulsion process is the ability to create particles as well as capsules with a defined properties under properly chosen reaction conditions (*i.e.*, physicochemical properties of the monomers/encapsulated materials and their corresponding ratios) (Mailander V, *et al.*, 2009). Polymerization

conditions had little influence on the final diameter while it severely affected the final molar masses of PBCA. An increase of the temperature and of the PH of the continuous phase led to higher molar masses. A further increase was observed when a radical initiator was added in the monomer (Hansali F, *et al.*, 2011).

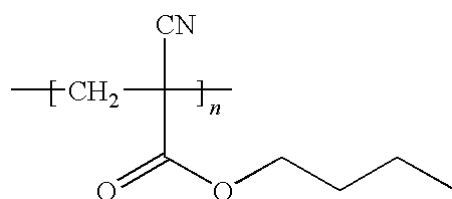


**Figure 5.** Chemical structure of PBCA

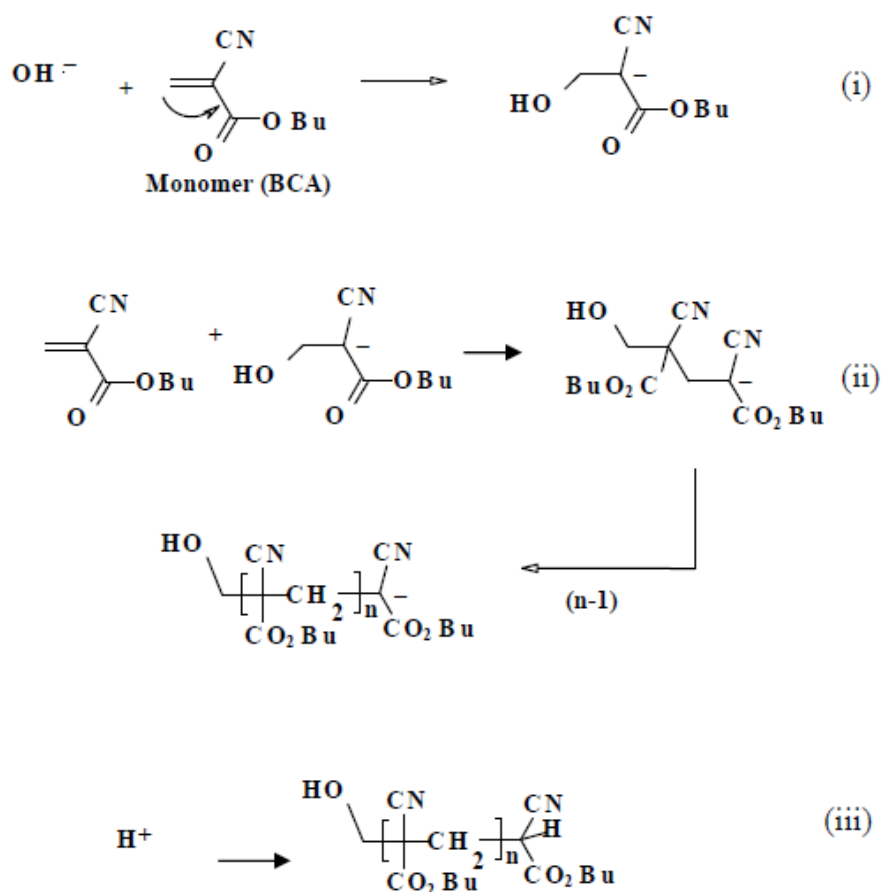


**Figure 6.** Polymerization mechanisms of PBCA. (i) Initiation; (ii) Growth; (iii) Termination.

Compared to the conventional emulsion, the mini-emulsion polymerization takes place in separated compartment, and the NPs can be produced under properly chosen reaction conditions. Surface modification and functionalization is carried out simultaneously or subsequently with appropriate pharmaceutical agents, fluorescent markers, various receptors, contrast agents, etc. The polymerization process is usually started by a radical or an anionic initiation reaction (in acidic medium). Thus, an oil phase (monomer n-butyl cyanoacrylate, soybean oil) is mixed with a water phase (phosphoric acid, surfactant) and homogenized by sonication at 0°C (mini-emulsion formation). Afterwards, the pH value is increased to about pH 7 by adding a base (ammonia) to polymerize the n-butyl cyanoacrylate.

### **1.5.3 Surface modification**

In our preliminary experiments, the combination of poloxamer 188 and DEAE-dextran was the most effective surfactant to enable BRB passage. Accordingly, for the current study I prepared poloxamer 188-modified, DEAE-dextran-stabilized (PDD) PBCA NPs with incorporated Rhodamine 123 by a mini-emulsion process. Surface modification with poloxamer 188 was carried out simultaneously with the polymerization process. Afterwards, different amounts of DEAE-dextran as stabilizer were added to produce the NPs with different surface charges. So from the inside to the outside, the structure of the PDD PBCA NPs is oil phase (with Rhodamine 123), polymeric surface with surfactant mask (Poloxamer 188), and stabilizer for adsorption equilibrium (DEAE-dextran).

## **1.6 Aims of the dissertation**

It is now widely accepted that the physiochemical properties of NPs, including

particle size, surface charge and surface hydrophilicity determine biological fate of NPs (Mosqueira VCF, *et al.*, 1999; Hans ML & Lowman AM, 2002; Thiele L, *et al.*, 2003). Yet, little is known of how physiochemical properties influence the BBB passage *in vivo* where – unlike *in vitro* – NPs’ interaction with peripheral compartments may influence the BBB passage. To learn more about the mechanisms and optimize NPs’ delivery potential, I reasoned that varying different parameters might shed some more light on the possible mechanisms of NPs’ actions. By comparing production protocols with different tensides and stabilizers, the prior work shows that the surfactant composition of PBCA NPs can have an “all-or-nothing” effect on their entry into brain tissue (Figure 7; Voigt N, *et al.*, 2014).

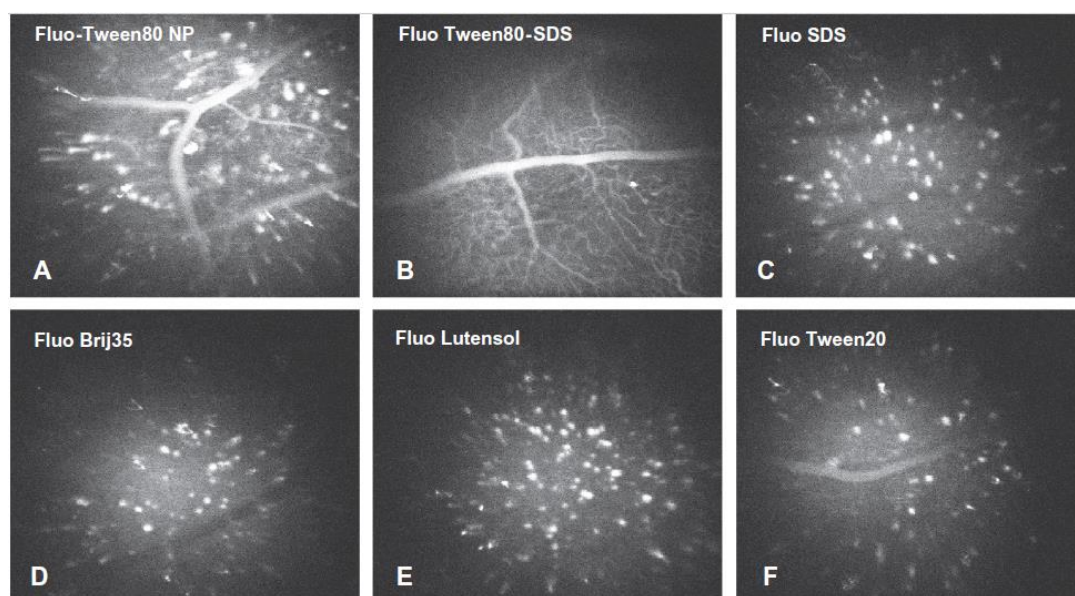


**Figure 7.** Nanoparticles with different surfactants (Voigt N, *et al.*, 2014). These microphotographs demonstrate that non-ionic tensides enables PBCA-NP to cross the BBB, whereas adding the anionic tenside SDS stops PBCA NP from entering the brain tissue (B). (A) (Tween80), (C) (SDS), (D) (Brij35), (E) (Lutensol) and (F) (Tween20): staining of cellular structures within the parenchyma 5–7 min after injection; (B) (Tween-SDS): staining of the cellular structure is not detectable 5–7 min after injection but there is clear staining of the blood vessels.



The current analyses were performed to further delineate optimal parameters of size and surface charge to achieve maximum entry into brain tissue.

1. The first aim of these analyses was to systematically study the influence of size and surface charge on BRB passage and analyze the kinetic profiles of the NPs by quantifying the fluorescent signals in retinal blood vessel and retina tissue. This is addressed in chapter 2.

2. The second aim was to study the retina of rats after *i.v.* injection of fluorescent NPs and imaged them *ex vivo* in retina tissue to determine the detailed location of NPs. This is addressed in chapter 3.

3. The hypothesis that the physicochemical parameters can influence NP's BBB passage not only by single up-take mechanisms but also by multiple *in vivo* ways such as interaction with blood constituents and peripheral compartments was analyzed. This is addressed in chapter 2 & 3.

The results presented in this dissertation should provide a better understanding of the “*in vivo*” kinetic of NPs and their cellular distribution by combining the *in vivo* and *ex vivo* approach.

## **2 Major effects on BRB passage kinetic by minor alterations in design**

### **2.1 Introduction**

The endothelial cells that make up the blood vessel walls separate the circulating blood from parenchyma, extracellular matrix and extracellular fluid. In the central nervous system, together with pericytes, glia endfeet and basal lamina, the endothelial cells are connected by tight junctions to form a highly selective membrane which comprises the blood-brain barrier (BBB) (Mayer F, *et al.*, 2009). It shields the brain tissue from unwanted molecules through different mechanisms that regulate the exchange of molecules, ions and even nanoparticles cross this barrier, including active transport based systems and diffusion based systems (Zhou Y, *et al.*, 2018). In this way the BBB is a “gate keeper” for metals, hormones, toxicants and neurotransmitters, thus ensuring a stable homeostasis which is critical as the neurons react quite sensitively to any changes in the extracellular milieu (Luissint AC, *et al.*, 2012). The downside of this tight control by the BBB is that it comprises a problem for most drugs as it prevents their passage into the brain. To overcome this limitation, many drug carriers were developed to deliver drugs across the BBB, in particular the biocompatible and biodegradable polymeric nanoparticles (NPs) like polybutylcyanoacrylate (PBCA) NPs since 1995 (Kreuter J, *et al.*, 1995; Alyautdin RN, *et al.*, 1998; Olivier JC, *et al.*, 1999). The fundamental approach was to mask the unfavorable physicochemical characteristics of the incorporated drugs and transport them across the BBB. Despite numerous studies showing the feasibility of this approach, the mechanisms of NP’s BBB passage are still unclear and little is known about the physicochemical parameters that enable or enhance the passage. To learn more about these mechanisms and optimize NPs’ delivery potential, I reasoned that varying different parameters might shed some more light on the possible mechanisms

of the actions.

One way to optimize the BBB passage of the NPs is to modify their surface as, for example, to allow receptor-mediated endocytosis in brain capillary endothelial cells (Gabathuler R, *et al.*, 2010; Wohlfart S, *et al.*, 2012; Zhou Y, *et al.*, 2018). Modifications of NPs' surface with covalently attached targeting ligands like apolipoprotein A-ligand (Kreuter J, *et al.*, 2007; Petri B, *et al.*, 2007) or coating NPs with surfactants like polysorbate 80 – which attracts a corona of plasma proteins - induce such receptor-mediated uptake (Wohlfart S, *et al.*, 2012). Despite these achievements, the *in vivo* efficacies of most NP modifications are still quite limited (Wang CX, *et al.*, 2009). By comparing production protocols with different tensides and stabilizers, our prior work shows that the surfactant composition of PBCA NPs can have an “all-or-nothing” effect on their entry into brain tissue. However, no systematic quantitative studies had been carried out to further delineate optimal parameters of size and surface charge to achieve maximum entry into brain tissue. But this knowledge is essential for the development of efficient and clinically useful NP systems.

To accomplish this goal, we systematically studied the NP composition parameters and their effects on entry into brain tissue using an efficient, reliable and non-invasive *in vivo* confocal neuroimaging system (Sabel BA, *et al.*, 1997; Rousseau V, *et al.*, 1999 and 2001; Prilloff S, *et al.*, 2007 and 2010; Henrich-Noack P, *et al.*, 2012; Voigt N, *et al.*, 2014; Khalid MK, *et al.*, 2018). Here, the fluorescent NP's passage across the blood retina barrier (BRB) can be visualized in the living rat with a confocal laser scanning microscope. The retina is the only brain tissue available for non-invasive *in vivo* microscopic imaging. Although the BRB is more permeable than the BBB for some compounds (Toda, *et al.*, 2011) and the trans-endothelial electrical resistance of the BRB *in vitro* reported by Campbell *et al.* is around  $50 \Omega/\text{cm}^2$  (Campbell M, *et al.*, 2011), which is lower than BBB *in vitro* over  $200 \Omega/\text{cm}^2$  (Freese C, *et al.*, 2017), the

BRB and BBB are similar regarding the expression of efflux proteins and the permeability for many drugs (Steuer H, *et al.*, 2004 and 2005). Regarding passage of NPs into brain tissue, the preliminary data suggest that the results from our BRB model are also valid for the situation at the BBB. I therefore use the eye as a “window to the brain”. With this model I visualize the function of the inner BRB which is being formed of the tight junctions between the retinal capillary endothelial cells (Cunha-Vaz J, *et al.*, 2011).

I chose PBCA NPs as promising polymeric drug carriers, as they have a well-characterized, good safety profile and have already been used in patient studies (Zhou Q, *et al.*, 2009). To visualize the NPs, I loaded them with the fluorescent agent Rhodamine 123 as a surrogate for an active compound. Being a substrate of P-glycoprotein (Jouan E, *et al.*, 2016), Rhodamine 123 does not cross the BRB in free form. Thus, the appearance of the fluorescence in the retina tissue unequivocally indicates the ability of the NPs to pass the BRB. After injecting the fluorescence-labeled NPs into the tail vein, the fluorescent signals in blood vessels and retina tissues can be visualized and semi-quantified in real-time and repeatedly over an extended period of time.

In our previous study, surfactant was found to be a critical factor determining the BRB passage of PBCA NPs (Voigt N, *et al.*, 2014); the combination of poloxamer 188 and DEAE-dextran was the most effective surfactant to enable BRB passage. Using this specific NP design, I now systematically studied the influence of size and surface charge on BRB passage and analyzed the kinetic profiles of the NPs by quantifying the fluorescent signals in retina blood vessel and retina tissue. In addition, the hypothesis that the physicochemical parameters can influence NP's BBB passage not only by single up-take mechanisms but also by multiple *in vivo* ways such as interaction with blood constituents was analyzed with *in vitro* incubation of the NPs and serum.

## 2.2 Materials and Methods

### 2.2.1 Equipments

Catheter	Adsyte Pro 22 G; BD, Heidelberg, Germany
Concave lens	KPC-013; Newport GmbH, Darmstadt, Germany
Microscopes	LSM 5 Pascal; Carl Zeiss AG, Jena, Germany
Microscope Workstations	LSM 5 Pascal v3.2 sp2; Carl Zeiss GmbH, Jena, Germany
Glass filter	800 µm pore size; Schott, Mainz, Germany
Head holder	Narishige Internation Ltd., London, UK
Spectrophotometer	Opsys MR; DYNEX Technologies
Ultrasonic homogenizer	Sonoplus HD 2070; Bandelin, Berlin, Germany
Zetasizer	Nano ZS; Malvern Instruments, Worcs., UK
Centrifuge	5804 R; Eppendorf AG, Hamburg, Germany

### 2.2.2 Reagents

Ammonia solution	Merck, Darmstadt, Germany
Chloral hydrate	7%; Fluka-Sigma Aldrich GmbH, Steinheim, Germany
DEAE-dextran	Sigma-Aldrich GmbH, Taufkirchen, Germany
Domitor	1.0 mg/ml medetomidine hydrochloride; Orion Corporation, Espoo, Finland
Ketavet	100 mg/ml ketamine hydrochloride; Zoetis Deutschland GmbH, Berlin, Germany
n-butyl- $\alpha$ -cyanoacrylate	Sicomet 6000; Henkel AG & Co.KG, Düsseldorf, Germany
Neosynephrine	POS 5%; URSAPHARM Arzneimittel GmbH, Saarbrücken, Germany

Phosphoric acid	Merck, Darmstadt, Germany
Poloxamer 188	Lutrol F68; BASF Ludwigshafen, Germany
Rhodamine 123	Sigma-Aldrich, Taufkirchen, Germany
Saline	Fresenius Kabi Germany, Bad Homburg, Germany
Soybean oil	Ph. Eur.; Roth, Karlsruhe, Germany
Vidisic optical gel	Bausch & Lomb, Berlin, Germany

### 2.2.3 Nanoparticle production

The PDD PBCA NPs with incorporated Rhodamine 123 were synthesized by a mini-emulsion process (Figure 8). Briefly, the O/W mini-emulsion was made from an aqueous phase and an oil phase. The aqueous phase, consisting of 0.2 g poloxamer 188, 0.01 g Rhodamine 123 and 4.5 ml of 0.1 M phosphoric acid, was allowed to stand at room temperature for 30 min and then placed into ice water for 5 min. The oil phase, consisting of 1.168 g n-butyl-2-cyanoacrylate and 0.045 g soybean oil, was added to the aqueous phase and then treated immediately with the ultrasonic homogenizer at 50% amplitude in ice water for 1 min. Afterwards, the mini-emulsion was added dropwise into 4.5 ml of 0.1 M ammonia solution and stirred at room temperature for 5 min. The pH value of the suspension was adjusted to 7.0 by adding more ammonia solution. Finally, DEAE-dextran was added into the suspension at different concentrations for producing NPs with distinct size and zeta-potential (Table 1) and stirred at room temperature for a duration of 30 min. The resulting NP suspension was filtered through a glass filter with a pore size of 800  $\mu\text{m}$  to remove NP agglomerates, then kept at a temperature of 4°C and protected from light until used in the experiment. The suspension was stored for a maximum of 10 h before injected into the rat tail vein.

For the Rhodamine 123-adsorbed NPs, 0.01 g Rhodamine 123 was added not to the aqueous phase but to the mini-emulsion after polymerization, and the suspension was

stirred at room temperature for 5 min.

For separating the small-size portion of NPs, the NP suspension was centrifuged at 9000 rpm for a duration of 10 min to remove the large-size NPs. I then tried to resuspend the large-size NPs in distilled water, which was, however, not possible because they agglomerated too much after centrifugation. Therefore, in my experiment I refer to “large” size as the original NP solution which was not centrifuged and therefore included the large size NPs as well as other fractions.

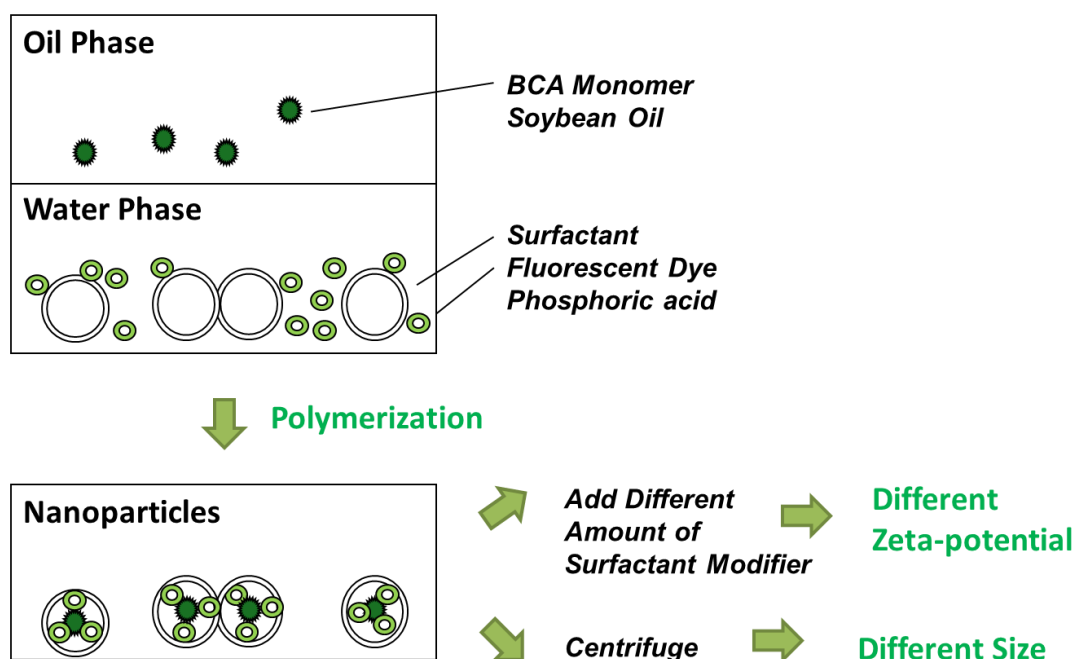


**Figure 8.** NP production and minor alterations in design

Six different NP variations were produced which systematically varied in size and surface charge (Table 1).

**Table 1.** Compositions of PDD PBCA NPs.

NP suspension	Labeling method	DEAE-dextran (g)	Centrifugation
Unlabelled	Unlabelled	0.09	No
Rhodamine 123-adsorbed	Adsorbed	0.09	No
Low-charge	Incorporated	0.01	No
Medium-charge	Incorporated	0.09	No
Medium-charge small-size	Incorporated	0.09	Yes
High-charge	Incorporated	0.2	No

The amount of following components for NP production were constant in each preparation: 0.2 g Poloxamer 188, 4.5 ml 0.1. M phosphoric acid, 1.168 g n-Butyl-2-cyanoacrylate and 0.045 g Soybean oil. (Definition of low-, medium-, high-charge see Table 4)

#### 2.2.4 Nanoparticle characterizations

Particle size, polydispersity index (PDI) and zeta-potential of NPs in the suspension were analyzed using a Zetasizer at 25°C. The NP suspension was diluted 1:20 with deionized water to eliminate primary charge effects.

The solid content of NP suspension was measured by drying the suspension at 70°C for 1 h and comparing the mass of the suspension and the mass of dried residuum.

The amount of bound Rhodamine 123 in NP suspension was calculated by determining the amount of free Rhodamine 123 in the supernatant by a spectrophotometer after a centrifugation at 12000 rpm for a duration of 10 min and subtracting it from the total amount of Rhodamine 123 in the suspension.

#### 2.2.5 Animals

Twenty six adult Lister hooded rats (CrI:LIS; Charles River) were kept on a 12-h light:



12-h dark cycle at an ambient temperature of 24–26°C at 50–60% humidity. Before NP injection, the rats were anaesthetized with an intraperitoneal injection of Ketavet (0.75 ml/kg) and Domitor (0.5 ml/kg). At the end of *in vivo* retina imaging experiments, all animals were killed by an over dose of chloral hydrate (0.35 g/kg).

For all procedures, ethical approval was obtained according to the requirements of the German National Act on the Use of Experimental Animals (Ethic committee Referat Verbraucherschutz, Veterinärangelegenheiten; Landesverwaltungsamt Sachsen-Anhalt, Halle, Germany; AZ42502-2-1150).

### **2.2.6 Co-incubation of nanoparticles and serum**

The fresh serum was prepared using the whole blood from the aorta of the rat. The blood was allowed to stand at room temperature for 1 h and kept at 4 °C for 24 h, then centrifuged at 3000 rpm for 10 min to get the supernatant serum. Finally, 0.9 ml NP suspension was co-incubated with 0.1 ml serum at 38 °C for 10 min. I used only 10% serum to avoid too much influence of proteins in the following analysis and observation of the NPs. NP solutions without co-incubation were set as control groups.

Particle size and PDI of the NPs in the suspensions were analyzed with 1:20 dilution with deionized water by Zetasizer Nano ZS directly without co-incubation and after starting the co-incubation and after 10 min.

A SEM was applied to visualize the effect of the 10 min co-incubation on the NPs. The pure NP suspension and serum co-incubated suspension were separately applied to the sample plate, freeze-dried and measured at 5 kV. Because time for sample processing is required before final measurement, it is impossible to get the image at the very beginning of co-incubation. Therefore I only compare the 10 min co-incubation group with control group.

### 2.2.7 Nanoparticle injection

Before NP application, the rats were anaesthetized with Ketavet/Domitor. The NP suspension was injected intravenously via the tail vein of rat with a single dose of 450  $\mu\text{g}$  NP-bound Rhodamine 123 per kilogram body weight using a pre-implanted catheter.

### 2.2.8 *In vivo* retina imaging and kinetic studies

*In vivo* retina imaging (Figure 10) was carried out before and at several time points after NP injection. Briefly, the eye of the anaesthetized rat was treated with Neosynephrin-POS 5% to dilate the pupil, and Vidisic optical gel was applied as an immersion medium for the contact lens and to protect the cornea from drying. After that, the rat was positioned underneath a confocal laser scanning microscope/LSM 5 Pascal with a large probe space and a long-working-distance objective lens. The eye was positioned directly underneath the objective lens with a Hruby style-80 dioptre plan concave lens onto the surface of the cornea to adjust the laser path. Using  $\times 5$  magnification, a  $2.6 \times 2.6 \text{ mm}^2$  well-defined area of the retina with clearly visible blood vessels was traced.



**Figure 10.** *In vivo* imaging of retina (from Prilloff S, *et al.*, 2010).

### 2.2.9 Image analysis

To compare the fate of the Rhodamine 123-incorporated NPs, the fluorescence signals in blood vessel and retina tissue were quantified over time by Image J/Fiji 1.46. Briefly, the images of each individual rat before and at several time points after injection were aligned to focus the analysis on the same area of the retina throughout the experiment. For blood vessels, the regions of interest (ROIs) were selected automatically by setting a threshold of grey value ( $\geq 80$ ) in the image taken 1 min after injection. For retina tissue, the ROIs were selected in the image 30 min after injection with the maximum fluorescence signals, but fluorescence signals of agglomerated NPs blocked in microvessels were excluded. Then the grey values of the same ROIs in aligned images were analyzed, and the concentrations of the NPs were calculated as percentage fluorescence intensity (FI) over background fluorescence by the following formula:

$$FI = (MGV - MGV_{\text{vessel } 0 \text{ min}}) / (MGV_{\text{background } 0 \text{ min}} - MGV_{\text{vessel } 0 \text{ min}}) \times 100 - 100$$

where the mean grey value (MGV) of blood vessels or retina tissues was determined by Image J. “ $MGV_{\text{vessel } 0 \text{ min}}$ ” corresponds to the mean grey value of the blood vessel in the image before injection as background noise-reference. “ $MGV_{\text{background } 0 \text{ min}}$ ” corresponds to the mean grey value of the retina tissue in the image before injection.

The variation induced in the FI in the background depends on the scanning acquisition conditions. So I used this value as a reference to avoid modification on the “MGV” induced by bleaching or other reasons.

### 2.2.10 Statistical analysis

All data were expressed as means  $\pm$  standard deviation ( $\bar{x} \pm s$ ) and analyzed by SPSS

Statistics 24.0 (IBM Corporation, NY, USA). The Size and PDI of the NPs at the beginning and after co-incubation with serum were compared in paired-samples t-test. The intensity of fluorescence signals after injection with the medium-charge NPs and the fraction of the medium-charge small-size NPs were compared in independent-samples t-test. The intensity of fluorescence signals after injection of low-charge, medium-charge and high-charge NPs were compared in one-way ANOVA with post hoc Tukey or Dunnett's T3.  $P < 0.05$  was considered statistically significant.

## 2.3 Results

### 2.3.1 Nanoparticle characterizations

Table 2 shows the characteristics of the six variations of PDD PBCA NPs which differ in size, surface charge and labeling method and was used for *in vivo* imaging and kinetic studies. By adding different amount of DEAE-dextran as stabilizer, zeta-potential can be varied in a range from 0 to 15 mV.

**Table 2.** Characterizations of PDD PBCA NPs (n = 5 batches,  $\bar{x} \pm s$ )

NP suspension	Z-average size (nm)	Zeta-potential (mV)	Bound Rhodamine 123 (mg/ml)	PDI	Solid content (%)
Unlabelled	160 ± 3	8 ± 1	0	0.22 ± 0.00	ND
Rhodamine 123-adsorbed	192 ± 4	3 ± 1	ND	0.16 ± 0.02	9.1 ± 0.3
Low-charge	272 ± 44	0 ± 1	0.45 ± 0.02	0.26 ± 0.03	9.6 ± 0.3
Medium-charge	272 ± 23	5 ± 2	0.44 ± 0.02	0.22 ± 0.02	9.2 ± 0.2
Medium-charge small-size	172 ± 10	3 ± 1	0.12 ± 0.02	0.10 ± 0.03	2.5 ± 0.2
High-charge	267 ± 13	15 ± 3	0.45 ± 0.01	0.24 ± 0.02	9.7 ± 0.3

ND: not determined

### 2.3.2 Degradation and agglomeration in blood

To understand the interactions of PDD PBCA NPs with blood, I co-incubated low-charge, medium-charge, medium-charge small-size and high-charge NP solutions with fresh rat serum at 38 °C for 10 min. I used only 10% serum, so proteins from

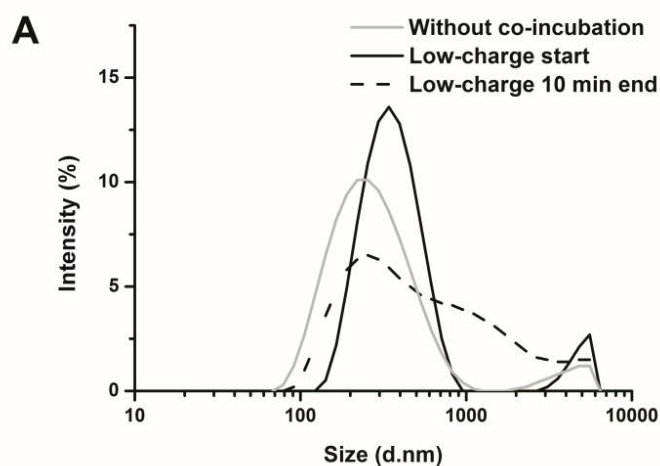
serum didn't influence the following analysis and observation of the NPs too much (Table 3 and Figure 10).

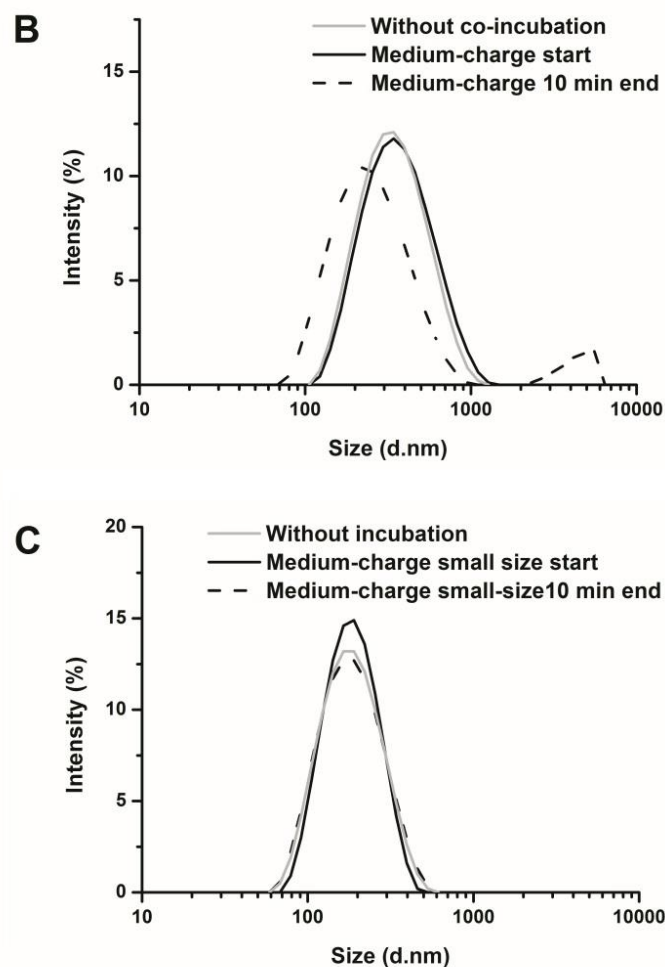
After 10 min of incubation, the size distribution of the low-charge NPs had changed considerably: the intensity of particles increased with Z-average size < 190 nm and decreased between 190 nm and 615 nm (Figure 10A). Interestingly, the intensity of particles size > 615 nm also increased and the amount of large agglomerated particles decreased (Figure 10A & 11A). This demonstrates that on one hand low-charge NPs could degrade in blood. On the other hand, as the averaged particle size and the PDI increased significantly (Table 3), it can be concluded that low-charge NPs both degraded and agglomerated. For medium-charge NPs, most particles became smaller which is indicated by a shift to the left in the size distribution graph, and the intensity of particle size <255 nm clearly increased (Figure 10B). At the same time, some very large agglomerated particles appeared (Figure 10B & 11B). Because the PDI remained constant (Table 3), it can be concluded that medium-charge NPs also degraded and agglomerated in blood, but at a rate slower than low-charge NPs. For small-size, medium-charge NPs, the morphology and the particle size distribution nearly didn't change (Table 3, Figure 10C & 11C). This shows small-size, medium-charge NPs to be relatively stable in blood. The high-charge NPs were too polydisperse to obtain meaningful data of particle size and PDI. However, SEM images indicate that the large agglomerated particles increased while most small particles disappeared (Figure 11D). This indicates that high-charge NPs degraded and agglomerated rather quickly in blood.

**Table 3.** Z-average size and PDI of PDD PBCA NPs at the start and the end of the 10 min co-incubation with serum (n = 3 batches,  $\bar{x} \pm s$ )

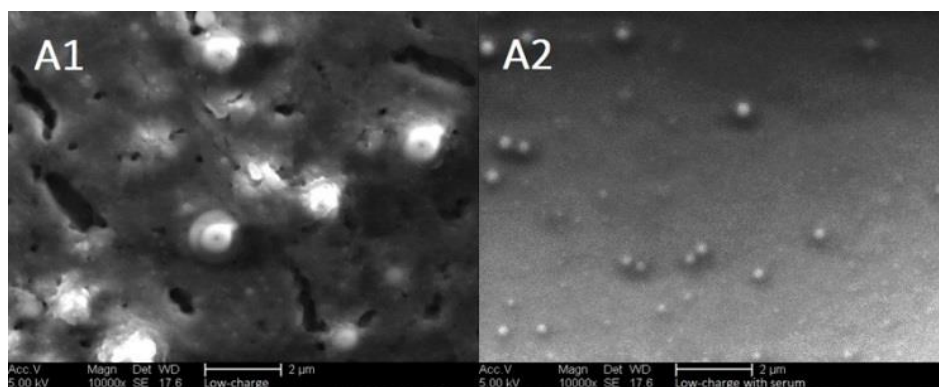
NP suspension	Without co-incubation		Start		End	
	Z-average size (nm)	PDI	Z-average size (nm)	PDI	Z-average size (nm)	PDI
Low-charge	287 ± 51	0.25 ± 0.01	331 ± 4	0.38 ± 0.01	357 ± 10*	0.45 ± 0.03*
Medium-charge	269 ± 26	0.21 ± 0.02	318 ± 26	0.21 ± 0.01	242 ± 7	0.29 ± 0.02
Medium-charge small-size	179 ± 8	0.08 ± 0.00	165 ± 4	0.13 ± 0.02	161 ± 4	0.16 ± 0.01
High-charge	270 ± 16	0.23 ± 0.01	NQ	NQ	NQ	NQ

NQ: can not be quantified. \*P < 0.05, compared between start and end





**Figure 10.** Representative particle size distribution of NPs at the start and end of 10 min co-incubation. PDD PBCA NPs were co-incubated with serum for 10 min and analyzed by Zetasizer Nano ZS. NPs without co-incubation were set as control groups.





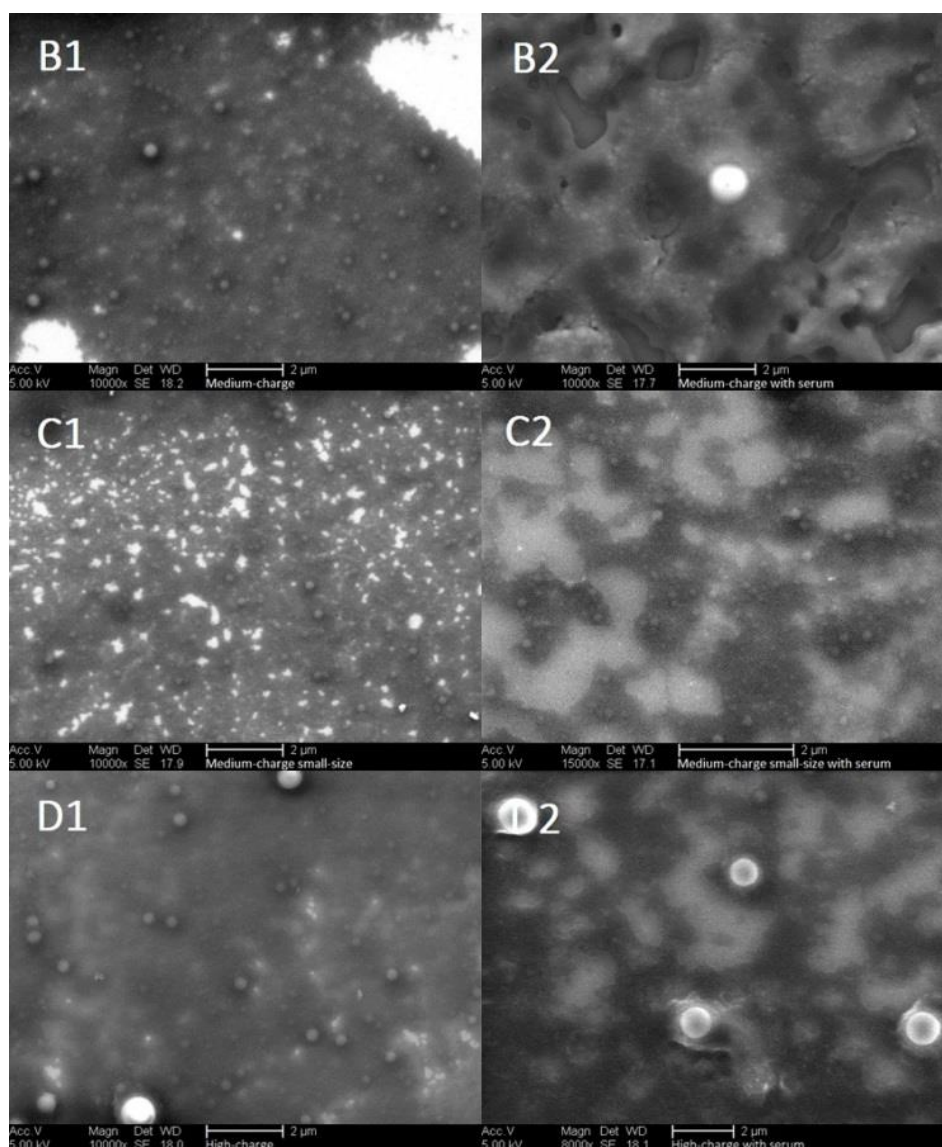


**Figure 11.** Morphology of NPs with or without co-incubation. Low-charge (A1), medium-charge (B1), medium-charge small-size (C1) and high-charge (D1) PDD PBCA NPs were measured by scanning electron microscope (SEM). After 10-min co-incubation with serum, they were measured again. For low-charge NPs (A2), the large agglomerated particles disappeared. For medium-charge NPs (B2), the large agglomerated particles appeared while most particles became smaller. For medium-charge small-size NPs (C2), their morphology nearly didn't change. For high-charge NPs (D2), the large agglomerated particles increased while most small particles disappeared.

### 2.3.3 No unspecific BRB opening

To learn whether PDD PBCA NPs passed the BRB via unspecific opening or specific transport, I injected unlabeled NPs followed by a separate injection of fluorescence dye (saline containing 0.45% Rhodamine 123) after 10 min and performed *in vivo* retina imaging. The fluorescence signals were strictly confined to the vessel lumen (Figure 12A) and detectable only within 5 min (Figure 12B). This experiment demonstrates that PDD PBCA NPs do not open the BRB unspecifically.

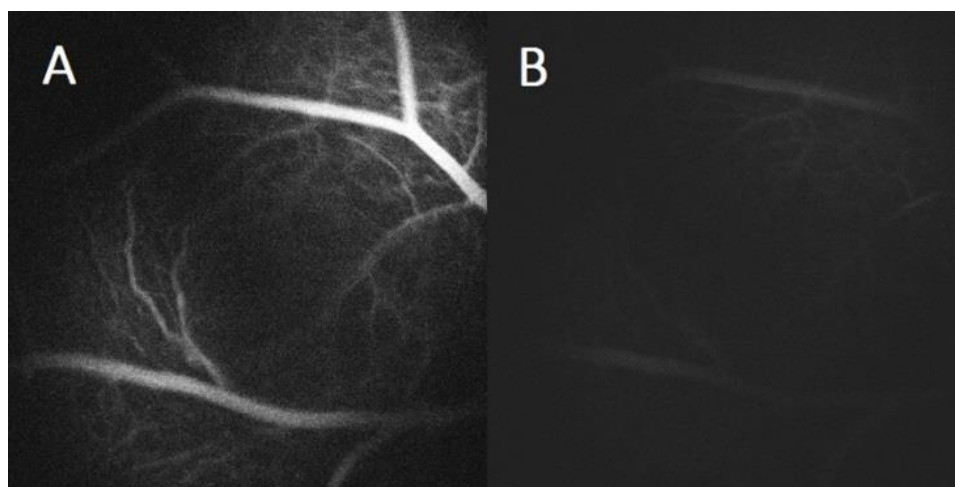


**Figure 12.** “BRB opening” test. I tested whether PDD PBCA NPs could open the BRB unspecifically by injecting Rhodamine 123 at 10 min after the injection of unlabeled NPs. The fluorescence signals were strictly confined to the vessel lumen (A) and detectable only within 5 min (B), which clearly shows that the BRB remained unaffected by the NPs.

### 2.3.4 Adsorbed labeling versus incorporated labeling

To compare the efficacy of adsorbed labeling *vs.* incorporated labeling, I injected Rhodamine 123-adsorbed or Rhodamine 123-incorporated (medium-charge) PDD PBCA NPs and performed *in vivo* retina imaging after 30 min. Rhodamine 123-incorporated NPs yielded more efficient fluorescence signals (Figure 13). This indicated that the incorporation labeling method was more suitable for subsequent

experiments.

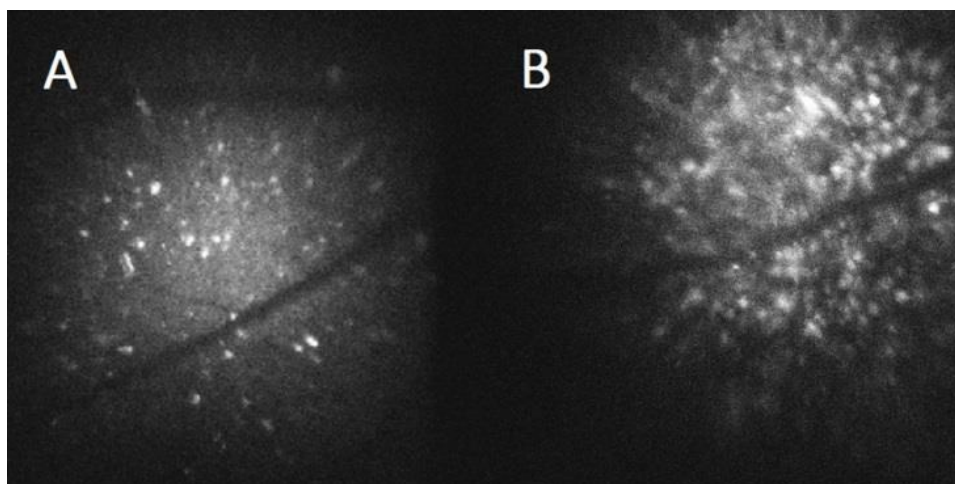


**Figure 13.** Adsorbed labeling vs. incorporated labeling. I tested whether adsorbed-labeled (A) or incorporated-labeled (B) PDD PBCA NPs yielded more efficient fluorescence signals after injection. The images demonstrate that 30 min after injection the retina tissue with Rhodamine 123-incorporated NPs were more fluorescent.

### 2.3.5 BRB passage kinetic

To visualize the kinetics of BRB passage, I injected PDD PBCA NPs and performed *in vivo* retina imaging before and at several time points after injection (Figure 14). A  $2.6 \times 2.6 \text{ mm}^2$  well-defined area of the retina with clearly visible blood vessels was traced. The fluorescence signals in blood vessels gradually decreased after the immediate peak post injection and almost disappeared within 30 min. At the same time, the fluorescence signals in retina tissue appeared after 5 min, then increased gradually, reaching a maximum value within 30 min, and were stable for at least 90 min, at which point the experiment ended. This indicates that poloxamer-DEAE-dextran PBCA NP could pass the BRB efficiently and the fluorescent marker remains in the retina tissue.

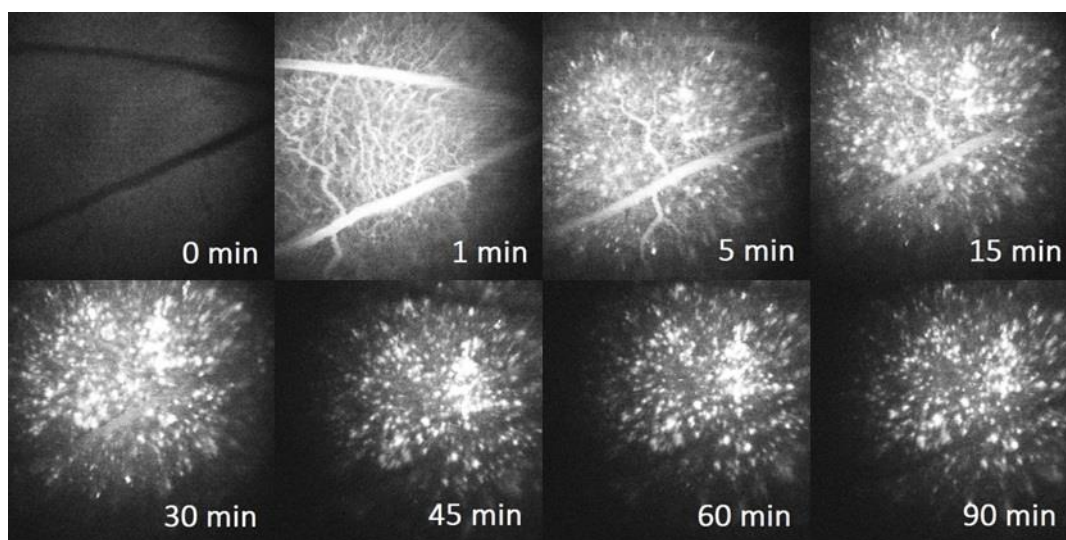


**Figure 14.** Representative images to demonstrate the NPs' kinetic of BRB passage. I injected medium-charge PDD PBCA NPs and performed *in vivo* imaging of the retina before and at several time points after injection. A  $2.6 \times 2.6 \text{ mm}^2$  well-defined area of the retina with clearly visible blood vessels was traced and efficient BRB passage was visualized.

### 2.3.6 Effects of surface charge

To determine whether the physicochemical parameter “surface charge” of the NPs affects the BRB passage kinetic, I injected low-charge (zeta-potential 0 mV), medium-charge (5 mV) and high-charge (15 mV) PDD PBCA NPs and performed *in vivo* imaging of the retina before and at several time points after injection (Figure 15). The injection dose is adjusted by the amount of NP-bound Rhodamine123 to make the fluorescence signals comparable. The fluorescence signals in blood vessels and retina tissue were traced over time and quantified as fluorescence intensity.

For low-charge NPs, the fluorescence signal in blood vessels quickly decreased within 5 min post injection. Medium-charge NPs yielded significantly stronger fluorescence signal in blood vessels than low-charge and high-charge NPs from 30 min post injection on, while they induced significantly stronger signals in retina tissue

at all time points. Thus, the physicochemical parameters “surface charge” affects the BRB passage potential of NPs.

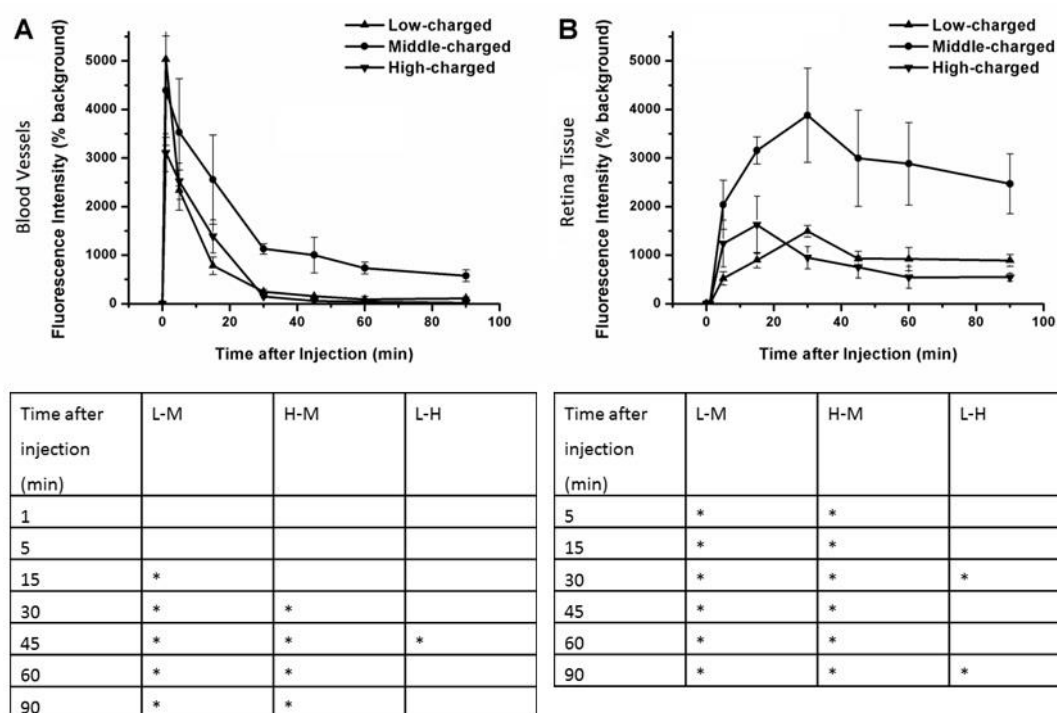


**Figure 15.** Kinetic profile of NPs with different surface charges ( $n = 5$ ,  $\bar{x} \pm s$ ). Tables beneath the line graphs show the statistical results of fluorescence intensity. L: low-charge. M: medium-charge. H: high-charge. \* $P < 0.05$ , compared between groups. Medium-charge (zeta-potential 6 mV) PDD PBCA NPs yielded significantly stronger fluorescence signals in blood vessel (A; from 30 min on) and retina tissue (B; all the time) than low-charge (0 mV) and high-charge (15 mV) NPs. This clearly shows that the factor “surface charge” affected the BRB passage of NPs.

### 2.3.7 Effects of size

To determine whether the physicochemical parameter “size” of the NPs affects the BRB passage kinetic, I injected original suspension (containing large and small particles; Z-average size 272 nm) and small-size fraction (after centrifugation of

original suspension; Z-average size 172 nm) of medium-charge PDD PBCA NPs and performed *in vivo* imaging of the retina before and at several time points after injection (Figure 16). The injection dose is adjusted by the amount of NP-bound Rhodamine123 to make the fluorescence signals comparable. The fluorescence signals in blood vessels and retina tissue were traced over time and quantified as fluorescence intensity.

Small-size portion of PDD PBCA NPs yielded significantly weaker fluorescence signals in both blood vessels and retina tissue. Thus, the physicochemical parameters “size” also affects the BRB passage potential of NPs.

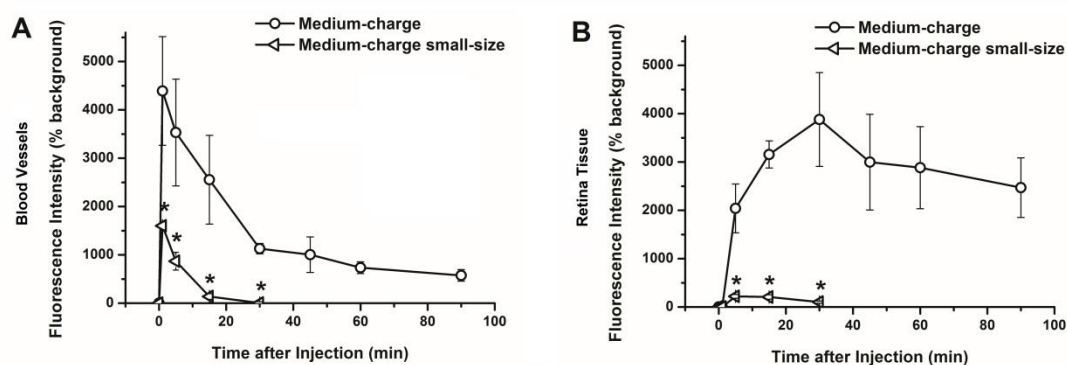


**Figure 16.** Kinetic profile of NPs with different sizes ( $n = 5$ ,  $\bar{x} \pm s$ ). \* $P < 0.05$ , compared between small-size portion and the original NP suspension. Small-size portion (Z-average size 172 nm) of PDD PBCA NPs yielded significantly weaker fluorescence signals in both blood vessel (A) and retina tissue (B) than the original NP suspension (272 nm).

## 2.4 Discussion

In order to study nanoparticles' passage across the BRB in living animals – a suitable surrogate model of the BBB – I carried out real-time imaging of blood vessels and retina tissue (Sabel BA, *et al.*, 1997; Rousseau V, *et al.*, 1999 and 2001; Prilloff S, *et al.*, 2007 and 2010; Henrich-Noack P, *et al.*, 2012; Voigt N, *et al.*, 2014; Khalid MK, *et al.*, 2018) before and several time points after intravenous injection. Whereas in our previous work on BRB passage of nanosystems we studied on the influence of different surfactants (Voigt N, *et al.*, 2014), I now have advanced my analysis to obtain semi-quantitative data on the kinetic profiles of fluorescence-labeled NPs, and I compared the NPs' BRB passage efficiency by determining the fluorescence signals in blood vessels and retina tissue.

Our earlier tests of different surfactants for NP production indicated that basically negatively as well as positively-charged PBCA NPs can cross the BRB and also larger size was not a hindrance as NPs with Z-average size of 130 nm and 422 nm yielded fluorescent signals in the tissue (Voigt N, *et al.*, 2014). However, for possible future applications as drug carriers, the most efficient nanoparticulate system needs to be identified. I therefore focused on optimizing the PDD PBCA NPs. This kind of NP was selected as it comprises the most promising variant from prior studies and pilot experiments.

In agreement with earlier observations I found the modification of the surface-coating-complex has a considerable influence on BRB passage of NPs: when altering the surface of the PDD NPs by adsorption of Rhodamine 123, the uptake into retina tissue was clearly lower than that of NPs with DEAE-dextran surfactant coating only where the Rhodamine 123 was incorporated (Figure 13). I therefore continued my experiments with the NPs which contained the incorporated Rhodamine 123 tracer and which were coated only with DEAE-dextran.

As a control experiment, I injected unlabeled NPs followed by a separate injection of fluorescence dye 10 min afterwards. *In vivo* imaging of the retina demonstrated that the fluorescence signals were strictly confined to the vessel lumen (Figure 12A) and detectable only within 5 min (Figure 12B). This demonstrates that PDD PBCA NPs do not open the BRB unspecifically, but is in contrast to the observations by Galla et al., who noticed a significant decrease in transendothelial electrical resistance of endothelial cells after incubation with PBCA nanoparticles (Galla HJ, 2018). Two possible reasons might explain this discrepancy. Firstly, the PDD PBCA nanoparticles I used have different surfactant, charge and size. Secondly, the *in vivo* retina model and the *in vitro* endothelial cell model are not comparable, reflecting different features and having different limitations with regard to the BBB.

It is known that after intravenous injection, most nanoparticles rapidly adsorb plasma components - mostly so-called opsonins – and, as a result, are rapidly cleared from the blood stream by the macrophages of the reticuloendothelial system of the liver and spleen. In mice the clearance of NPs after intravenous injection occurs already within 5 min (Pardridge WM, 1992). In my control experiment with Rhodamine 123 injection I observed that the dye, which is not bound to NPs, has also mostly disappeared from the vasculature within this time frame (Figure 12). The modification of the NP surface with covalent attachment of polyethylene glycol chains to the core polymer (Brigger I, *et al.*, 2002) can considerably prolong their blood circulation time and alter the body distribution significantly. This has also implications for brain delivery (Tiwari SB, *et al.*, 2006), as longer circulation time facilitates uptake. In my study, after tail vein injection of the PDD PBCA NPs, I observed a clearance of NPs from the retina blood vessels within 30 min. This was not noted after injection of the medium-charge group, which showed significantly higher fluorescence intensity in the vasculature than the low- and high-charge group during this 30 min period and beyond. Notably, however, the small-size fraction of the medium-charge NPs revealed the lowest signal in the vessels. This was already



detected at the moment of the injection. Moreover, the fluorescent signal of this NP group disappeared fastest (Figure 15 and Figure 16). Therefore I conclude that a larger size of medium-charge PDD PBCA NP allows prolonged circulation time as compared to its small size variant. The short circulation time may also be the reason underlying the very low BRB passage of the small-sized particles. Preliminary data from biopsies indicate an accumulation of NPs in lung and liver within 5 min after injection. Of note, this is especially pronounced for the accumulation of the small-size portion of medium-charge NPs in lung tissue (data shown in chapter 3). Therefore, I propose that after intravenous injection, reaching the heart and being pumped to the lung tissue, the NPs are subject to a kind of “first pass” effect where the small-sized NPs – not the larger ones - can “leak” through the fenestrated vessel walls of the lung’s veins and arteries. Therefore, it seems that size can influence NPs’ kinetic from the very beginning after entering into the blood system.

The quantification of the PDD PBCA NP with similar size but different surface charge suggested that the latter also significantly influences BRB passage. To understand the possible mechanisms, I therefore investigated the interactions of PDD PBCA NPs with blood. I co-incubated the particles with serum and analyzed size distribution with the Zetasizer Nano ZS and visualized NPs with a SEM. Zetasizer Nano ZS and SEM showed similar results (Table 3 and Figure 10). Surface charge and size considerably influenced the degradation and agglomeration speed of the NPs in the blood. A small portion of the low-charge NPs was found to be decreased in size after 10 min of serum incubation, probably indicating degradation. However, unlike the medium-charge NPs, I noticed a large fraction of the low-charge NPs which had increased in size. I assume that there was not enough repulsive force to keep stability, and the NPs started to agglomerate (Figure 11). The SEM images indicate that the high-charge NPs virtually disappeared after 10 min incubation in serum. One possible explanation is that this positive charge facilitates an interaction with negatively-charged serum-components like albumins which may facilitate

solubilization. Stein and Hamacher also carried out degradation tests on PBCA nanoparticles in dog serum, and almost complete hydrolysis was observed within 3.5 h (Stein M, *et al.*, 1992).

So far, research projects on BRB passage of NPs have indicated that surfactants are a key factor for successful brain delivery. Among the surfactants investigated, Tween 80 has long been considered to represent a ‘gold standard’ for effective brain delivery of PBCA NPs (Kreuter J, *et al.*, 2003). In the current work I used nonionic poloxamer 188 as surfactant. Both Tween 80 and poloxamer 188, being rather different in their chemical structures, still show very similar plasma protein adsorption patterns on PBCA NPs loaded with doxorubicin, with a remarkably high amount of apolipoprotein A, the major apolipoprotein component of high density lipoproteins (Petri B, *et al.*, 2007). It is known that the poloxamers - block-copolymers of poly (propylene oxide) and poly (ethylene oxide) – interact with cell membranes and, in particular, with lecithin, their essential component (Zhirnov AE, *et al.*, 2005). It was suggested that the preferred brain uptake of nanoparticulate systems with such surfactants are due to an affinity to lecithin and Apolipoproteins (Kreuter J, *et al.*, 2007). Therefore it is possible that coating with poloxamer 188 can assist these kinds of receptor-mediated uptake. However, my PDD NPs appeared in the retina tissue 5 min after injection and the peak concentration was achieved 30 min after injection (Figure 14). The passage through the BRB was too fast to consider only receptor-mediated uptake. Gulyaev *et al.* showed that the peak concentration of the doxorubicin loaded in the Tween 80-coated PBCA NPs in the rat brain was achieved 2 h after intravenous injection (Gulyaev AE, *et al.*, 1999), which is the typical time course for receptor-mediated uptake. In addition, I used cationic DEAE-dextran as stabilizer. As a widely-used transfection reagent, it binds negatively-charged DNA to form a complex which can be taken up by cells via adsorptive endocytosis (Smale ST, *et al.*, 2010). Therefore I assume that endocytosis may be the mechanism for the passage of my PDD PBCA NPs across the negatively-charged BRB. In this respect,

also the size may affect the endocytotic uptake mechanism. Generally, clathrin-mediated endocytosis was suggested to be the predominant pathway for the uptake of small particles below 200 nm, whereas the uptake of larger particles up to a size of 500 nm seems to be caveolae-mediated (Hillaireau H, *et al.*, 2009).

In conclusion, my current results demonstrate that for designing PDD PBCA NPs aimed at BRB and possible BBB passage it is unfavorable to have a small Z-average size below 200 nm, a high zeta-potential of 15 mV or a low one of 0 mV. My data indicate that this may be due to solubilisation, aggregation and peripheral uptake of these nano-systems before they can interact with the BRB. However, middle-sized PDD PBCA NP (272 nm) with an zeta-potential of 5 mV resulted in a highly efficient BRB passage. When taken together, and in view of other studies on the influence of different surfactants, I learned from my findings that none of the parameters, surfactant, size or surface charge can alone sufficiently determine if a given NP can pass the BRB. Only the combination of all these factors can predict the NP's post-injection behavior, like the interaction of nano-systems with each other, with blood components, with peripheral organs and with the BRB. Apparently, there are no standard rules for the design of nanoparticulate carriers for brain delivery; each nano-system requires its own design and optimization. In case of PDD PBCA NP, larger size and a medium zeta-potential were found to be the preferred variant to achieve BRB passage. More research is needed to further explore the feasibility and versatility of nanoparticles as possible vehicles for drug delivery.

### **3 Physicochemical parameters affect distribution in CNS via systematic interactions**

#### **3.1 Introduction**

It is now widely accepted that the physiochemical properties of NPs, including particle size, surface charge and surface hydrophilicity determine the biological fate of NPs (Mosqueira VCF, *et al.*, 1999; Hans ML & Lowman AM, 2002; Thiele L, *et al.*, 2003). Yet, little is known on how physiochemical properties influence the BBB passage *in vivo* where – unlike *in vitro* – NPs' interaction with blood and peripheral compartments may limit the BBB passage.

The standard method for analysing pharmacokinetic parameters of the BBB passage is the *in vivo* method of the “brain/plasma ratio” (Reichel A, 2006). Other techniques are “in situ brain perfusion”, “brain uptake index” or microdialysis (Elmqvist WF, *et al.*, 1997; Dagenais C, *et al.*, 2005). However, these techniques are rather complex, laborious and costly which limits their use for drug testing. We previously presented a rat model of *in vivo* retina imaging to study the influence of physiochemical properties on the BBB passage by comparing the *in vivo* kinetic of NPs (Voigt N, *et al.*, 2014; You Q, *et al.*, 2018).

In many studies, small size was found to be beneficial for BBB passage of NPs (Wohlfart S, *et al.*, 2012; Zhou Y, *et al.*, 2018). It has also been suggested that the size limitation for movement of NPs, *i.e.*, by diffusion, in the extracellular space is 64 nm maximum (Thorne RG, *et al.*, 2006). For Tween 80 coated NPs, the recommended size for the BBB passage is below 100 nm (Gao K, *et al.*, 2006). In contrast to this, our previous experiments demonstrated that the smallest PBCA NP modified with poloxamer 188-SDS (Z-average size 87 nm) was not effective to pass the BRB, whereas the very large NP modified with DEAE-dextran-poloxamer 188 (464 nm)

passed the BRB efficiently as well as the middle-sized NPs modified with Tween 80 (143 nm) (Voigt N, *et al.*, 2014). With reference to surface charge, negative charge has regularly been demonstrated to be beneficial for BBB passage of NPs (Zhou Y, *et al.*, 2018), but higher internalization rates are associated with positively-charged NPs because of the negatively-charged cell membrane composition (Wohlfart S, *et al.*, 2012). Regarding the passage into brain tissue, however, our former *in vivo* experiments showed that the positively-charged PBCA NP modified with Tween 80-dextran (zeta-potential 5 mV) and DEAE-dextran (20 mV) passed the BRB efficiently as well as the NP modified with Tween 80 (-26 mV) and poloxamer 188-dextran (-16 mV) (Voigt N, *et al.*, 2014). I hypothesized that the physicochemical parameters can influence NP's BBB passage not only by single up-take mechanisms but also by multiple *in vivo* ways such as interaction with blood constituents and peripheral compartments.

Further pilot experiments suggested that the combination of poloxamer 188 and DEAE-dextran was the most effective surfactant to enable BRB passage. Accordingly, for the current study I prepared poloxamer 188-modified, DEAE-dextran-stabilized (PDD) PBCA NPs with incorporated Rhodamine 123 by a mini-emulsion process. Surface modification with poloxamer 188 was carried out simultaneously with the polymerization process. Afterwards, different amount of DEAE-dextran as stabilizer were added to produce the NPs with different surface charges. For further separating the small-size portion of the NPs, the final suspension was centrifuged to remove the large-sized NPs. Being a substrate of P-glycoprotein (Jouan E, *et al.*, 2016), Rhodamine 123 does not cross the BRB in free form. After *i.v.* injection, the fluorescence signals in blood vessels gradually decreased after the immediate peak post injection and almost disappeared within 30 min. At the same time, the fluorescence signals in retina tissue appeared after 5 min, then increased gradually, reaching a maximum value within 30 min, and were stable for at least 90 min, at which point the experiment ended.

In the present study I now wish to further clarify the relationship of NP size and charge in our *in vivo* retina imaging model by studying the relationship of the zeta-potential 0, 5, and 15 mV and NPs sized 172 vs. 272 nm and its effects of BRB passage. To this end I now studied the retina of rats 30 min after *i.v.* injection of fluorescent NPs and imaged them *ex vivo* in retina tissue to determine the detailed cellular location of NPs by performing double and triple labelling. In line with prior *in vivo* kinetic results, I found that the NPs with larger size and medium surface charge accumulated more readily in brain and retina tissue. As in the current study, I also collected the blood and tissue samples from brain, heart, kidney, liver, lung and spleen, I could link the results of BRB passage with the accumulation of NP variations in the different organs. This combination of the “*in vivo*” kinetic and the “*ex vivo*” detailed distribution leads to a better understanding of the influence and mechanism of physicochemical features on NPs barrier passage and biodistribution, with which the hypothesis that the physicochemical parameters can influence NP’s BBB passage not only by single up-take mechanisms but also by multiple *in vivo* ways such as interaction with blood constituents and peripheral compartments was verified.

## 3.2 Materials and Methods

### 3.2.1 Equipments

Catheter	Adsyte Pro 22 G; BD, Heidelberg, Germany
Microscopes	LSM 880; Carl Zeiss AG, Jena, Germany
Microscope Workstations	ZEN 2.3 v14.0.0.201 sp1; Carl Zeiss GmbH, Jena, Germany
Glass filter	800 µm pore size; Schott, Mainz, Germany
Homogenisator	VDI 12; VMR, Leuven, Belgium
Spectrophotometer	Opsys MR; DYNEX Technologies
Stereotactic instrument	Digital Lab Standard Stereotaxic System; Hugo Sachs Elektronik-Harvard Apparatus GmbH, March-Hugstetten, Germany
Syringe for injection	10µl Hamilton; Sigma-Aldrich GmbH, Taufkirchen, Germany
Ultrasonic homogenizer	Sonoplus HD 2070; Bandelin, Berlin, Germany
Zetasizer	Nano ZS; Malvern Instruments, Worcs., UK
Centrifuge	5804 R; Eppendorf AG, Hamburg, Germany 1K15; Sigma-Aldrich GmbH, Taufkirchen, Germany

### 3.2.2 Reagents

4% paraformaldehyde solution	Otto Fischar GmbH & Co. KG, Saarbrücken, Germany
Ammonia solution	Merck, Darmstadt, Germany
Carboxylate-modified microspheres	0.04 µm, red fluorescent; Invitrogen GmbH, Karlsruhe, Germany

DEAE-dextran	Sigma-Aldrich GmbH, Taufkirchen, Germany
Domitor	1.0 mg/ml medetomidine hydrochloride; Orion Corporation, Espoo, Finland
Hoechst 33342	Cayman Chemicals, Hamburg, Germany
Ketavet	100 mg/ml ketamine hydrochloride; Zoetis Deutschland GmbH, Berlin, Germany
Methanol	Merck, Darmstadt, Germany
n-butyl- $\alpha$ -cyanoacrylate	Sicomet 6000; Henkel AG & Co.KG, Düsseldorf, Germany
Phosphoric acid	Merck, Darmstadt, Germany
Poloxamer 188	Lutrol F68; BASF Ludwigshafen, Germany
Proparacain	POS 0.5%; Ursapharm Arzneimittel GmbH & Co. KG, Saarbrücken, Germany
Rhodamine 123	Sigma-Aldrich, Taufkirchen, Germany
Saline	Fresenius Kabi Germany, Bad Homburg, Germany
Soybean oil	Ph. Eur.; Roth, Karlsruhe, Germany
Vidisic optical gel	Bausch & Lomb, Berlin, Germany

### 3.2.3 Animals

Twenty adult Lister hooded rats (320-400 g, CrI:LIS; Charles River) were kept on a 12-h light: 12-h dark cycle at an ambient temperature of 24-26°C at 50–60% humidity.

For all procedures, ethical approval was obtained according to the requirements of the German National Act on the Use of Experimental Animals (Ethic committee Referat Verbraucherschutz, Veterinärangelegenheiten; Landesverwaltungsamt



Sachsen-Anhalt, Halle, Germany; AZ42502-2-1283).

### 3.2.4 RGC labeling

To visualize the RGCs, retrograde labeling (Figure 17; Sabel BA, *et al.*, 1997; Prilloff S, *et al.*, 2010; Henrich-Noack P, *et al.*, 2012; Voigt N, *et al.*, 2014; Khalid MK, *et al.*, 2018) was carried out one week before NP injection. Before surgery, the rats were anaesthetized with an intraperitoneal injection of Ketavet (0.75 mL/kg) and Domitor (0.5 mL/kg). Two  $\mu$ l carboxylate-modified microspheres with red fluorescence were injected stereotactically into the left and right superior colliculus where the axons of the RGCs terminate. The coordinates were anterior-posterior 6.9 mm and lateral 1.2 mm. On the vertical axis four injections of 0.5  $\mu$ l each were made at 4.0, 3.5, 3.0 and 2.5 mm below the dura. Approximately 20 sec were allowed to elapse between each injection to facilitate dye diffusion.

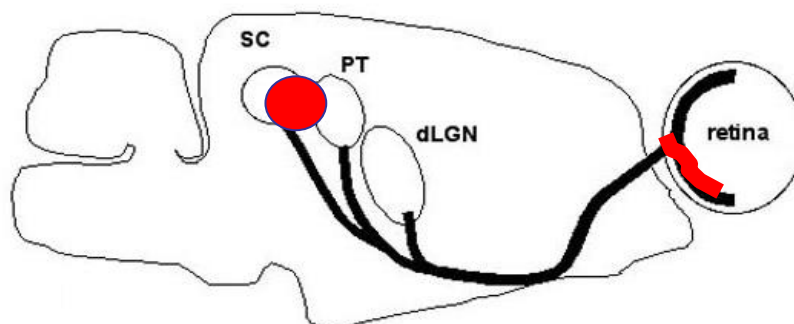


**Figure 17.** Retrograde labeling of RGCs by injecting a fluorescent dye into the superior colliculus.

### 3.2.5 Nanoparticle production

See chapter 2.2.3. The amount of Rhodamine 123 was adjusted from 0.01 to 0.008 g.

### **3.2.6 Nanoparticle characterization**

See chapter 2.2.4. In addition, all groups of PDD PBCA NPs were incubated with serum and the release rate of Rhodamine 123 was calculated.

### **3.2.7 Nanoparticle injection**

See chapter 2.2.7.

### **3.2.8 *Ex vivo* retina imaging and biodistribution studies**

Thirty min after NP injection, the rats were decapitated. The eyes were enucleated and placed in cold HEPES-buffered  $\text{Ca}^{2+}$ -free solution. The excess of connective tissues and muscles were removed, and the cornea was removed by cutting the rim with the sclera. After the lens and the vitreous were removed, the retina was separated from the pigment epithelium. To flatten the retina, four small cuts from edge directed to the optic nerve were performed. The retina was fixed with 4% paraformaldehyde solution for 10 min, washed with HEPES-buffered  $\text{Ca}^{2+}$ -free solution for three times, then stained by 5  $\mu\text{g}/\text{ml}$  Hoechst 33342 solution. Finally, the retina (Figure 18) was imaged using a confocal laser scanning microscope/LSM 880 at a 5 $\times$  and 50 $\times$  magnification. Hoechst 33342 was excited at 355 nm and detected at 420-495 nm. Rhodamine 123 was excited at 488 nm and detected at 496-565 nm. Red fluorescent carboxylate-modified microspheres were excited at 561 nm and detected at 566-640 nm.

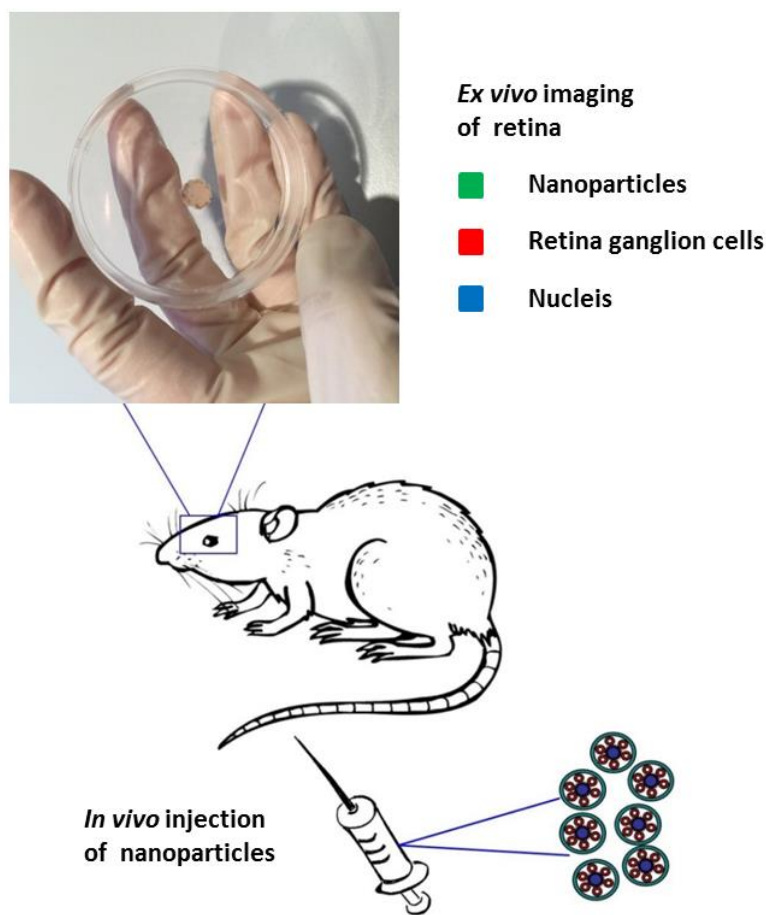


**Figure 18.** *Ex vivo* imaging of retina.

### 3.2.9 Biodistribution in brain and peripheral organs

After the rats were decapitated and eyes were enucleated, 2 ml blood was collected and the brain, heart, kidneys, liver, lungs and spleen were removed and cleaned with saline. The whole organs were weighted immediately after removal, 0.8 g small pieces of each organ were exactly weighed into centrifuge tubes. 2 ml saline was added and the tissues were homogenized by a homogenisator.

Rhodamine 123 standard was dissolved in saline to prepare 200  $\mu\text{g}/\text{ml}$  standard solution. Then the standard solution was added to blood or organ homogenates to prepare standard series with the concentration of 1.25 – 20  $\mu\text{g}/\text{ml}$  (Table 4).

**Table 4.** Preparations of standard series.

Concentration of Rhodamine 123 ( $\mu\text{g/ml}$ )	20	10	5	2.5	1
Volume of standard solution ( $\mu\text{l}$ )	200	100	50	25	10
Volume of tissue solution or blood ( $\mu\text{l}$ )	1800	1900	1950	1975	1990

The samples or standard series of blood or the homogenates were centrifuged at 5000 rpm for a duration of 5 min. 500  $\mu\text{l}$  supernatant was added into 1500  $\mu\text{l}$  methanol, vortexed for a duration of 5 min and centrifuged at 12000 rpm for a duration of 10 min. The final supernatant was dried and reconstituted in 100  $\mu\text{l}$  water, and the absorbance value of Rhodamine 123 was determined by a spectrophotometer. The relationship between the concentrations of Rhodamine 123 in blood or organ homogenates ( $X$   $\mu\text{g/ml}$ ) and the absorbance value of Rhodamine 123 ( $Y$ ) was regressed. There was good liner relationship over a range of 1.3 – 20  $\mu\text{g/ml}$  for concentrations of Rhodamine 123 in blood or organ homogenates (Table 5).

**Table 5.** Linear regression equations of concentrations of Rhodamine 123 in blood or organ homogenates.

Organ homogenates	Regression equations	$R^2$
Blood	$Y = 0.193 X + 0.0165$	0.9968
Brain	$Y = 0.192 X + 0.0114$	0.9991
Heart	$Y = 0.193 X + 0.0210$	0.9910
Kidneys	$Y = 0.190 X + 0.0371$	0.9929
Liver	$Y = 0.191 X + 0.0164$	0.9955
Lungs	$Y = 0.192 X + 0.0105$	0.9989
Spleen	$Y = 0.194 X + 0.0300$	0.9934

The amount of NPs distributed in blood or organs was calculated as percentage

injected dose per gram organ weight (% dose/g tissue) by the following formula:

$$\text{Amount of NPs} = C \cdot V / (D \cdot W) \times 100$$

where “C” corresponds to the concentration of Rhodamine 123 in blood or organ homogenates ( $\mu\text{g/ml}$ ). “V” corresponds to the volume of blood or organ homogenates (2 ml). “D” corresponds to the injected dose of NP-bound Rhodamine 123 (450  $\mu\text{g/kg}$ ). “W” corresponds to the body weight of rat (kg).

### **3.2.10 Statistical analysis**

All data were expressed as means  $\pm$  standard deviation ( $\bar{x} \pm s$ ) and analyzed by SPSS Statistics 24.0 (IBM Corporation, NY, USA). Biodistribution of medium-charge NPs and the fraction of medium-charge small-size NPs were compared in independent-samples t-test. Biodistribution of low-charge, medium-charge and high-charge NPs were compared in one-way ANOVA with post hoc Tukey or Dunnett's T3.  $P < 0.05$  was considered statistically significant.

### 3.3 Results

#### 3.3.1 Nanoparticle characterizations

Table 6 shows the characteristics of the four NP variations used for *ex vivo* imaging of retina and biodistribution studies. By adding different amounts of DEAE-dextran as stabilizer, zeta-potential can be varied in a range from 1 to 16 mV. For all variations of PDD PBCA NPs, Z-average size was found to be stable for at least 8 days (Figure 19). The bound rate of Rhodamine 123 was stable in the first day (Figure 20), and the release rate in serum was under 25% within the first 0.5 h (Figure 21). Thus, the appearance of the fluorescence in the retina tissue unequivocally indicates the ability of the NPs to pass the BRB.

**Table 6.** Characterizations of PDD PBCA NPs (n = 3 batches,  $\bar{x} \pm s$ ).

NP suspension	Z-average size (nm)	Zeta-potential (mV)	Bound Rhodamine 123 (mg/ml)	PDI	Solid content (%)
Low-charge	303 ± 4	1 ± 0	0.42 ± 0.03	0.31 ± 0.02	9.1 ± 0.3
Medium-charge	306 ± 4	4 ± 1	0.45 ± 0.04	0.27 ± 0.01	9.2 ± 0.2
Medium-charge small-size	154 ± 1	5 ± 0	0.14 ± 0.01	0.10 ± 0.00	2.6 ± 0.1
High-charge	336 ± 2	16 ± 0	0.46 ± 0.03	0.28 ± 0.01	9.8 ± 0.4

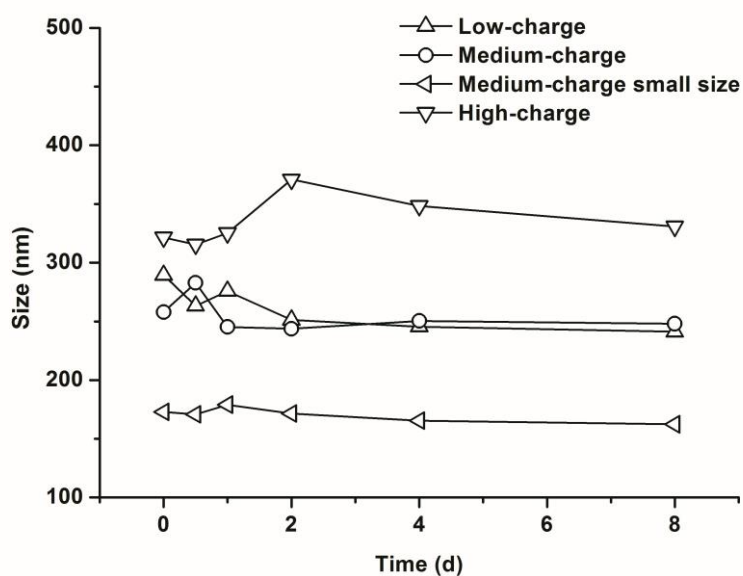


**Figure 19.** Stability of PDD PBCA NPs. For all variations of NPs, Z-average size was found to be stable for at least 8 days.

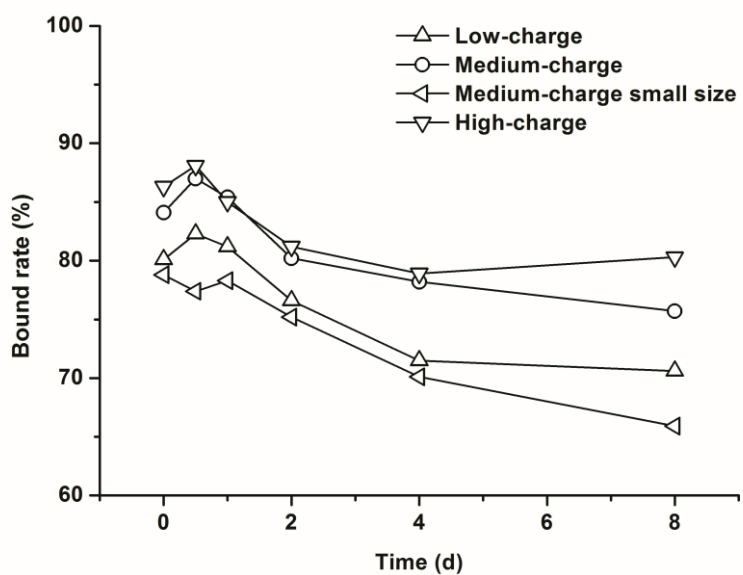


**Figure 20.** Bound rate of Rhodamine 123. For all variations of PDD PBCA NPs, the bound rate of Rhodamine 123 was stable in the first day and then gradually decreased until 8 days.

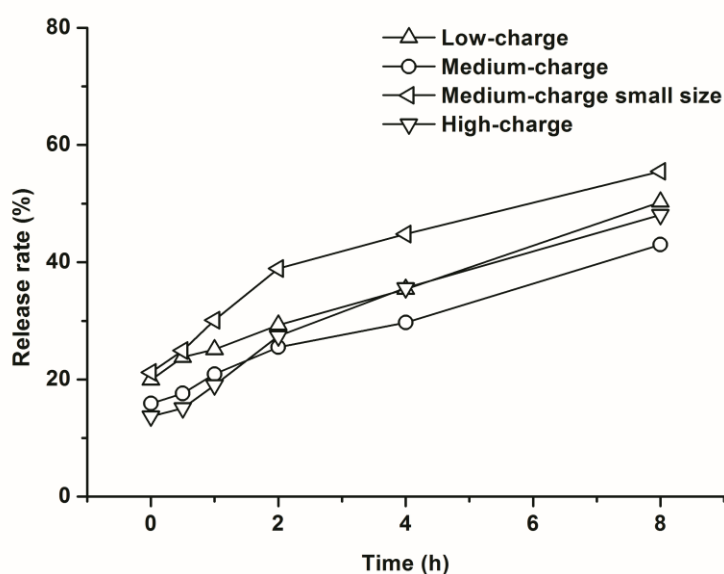


**Figure 21.** Release rate of Rhodamine 123. All variations of PDD PBCA NPs were incubated with serum and the release rate of Rhodamine 123 was under 25% within the first 0.5 h.

### 3.3.2 Biodistribution in retina cells

To visualize how the physicochemical parameters “surface charge” and “size” affect the detailed distribution of NPs in retina, I injected four variations of PDD PBCA NPs and performed *ex vivo* imaging of fluorescence signals in retina tissue 30 min after i.v. injection of NPs (Figure 23 & 24). The injection dose was adjusted to the amount of NP-bound Rhodamine123 to make the fluorescence signals comparable. RGCs were retrograde labeled with carboxylate-modified microspheres in red. Nuclei were stained with Hoechst 33342 in blue. NPs were labeled with Rhodamine 123 in green. In the 50× magnified images, co-localization of green and red signals indicates that the NPs were internalized by RGCs (Figure 24), and the percentage of RGCs with accumulated NPs over total amount of RGCs was calculated (Figure 22).

The low-charge NPs accumulated unevenly in the vessel walls and some



agglomerates attached on the surface of the vessel walls (Figure 23A & 24A1; Arrows). Most of the fluorescence signals distributed inside the cells remained outside of nuclei (Figure 24A3; Arrows). The medium-charge NPs yielded stronger fluorescence signals in the blood vessels (Figure 23B; Arrows) and more evenly distributed fluorescence signals in the retina tissue (Figure 24B1) than the low-charge and high-charge NPs. Over 70% of RGCs showed fluorescence signals of accumulated medium-charge NPs (Figure 22), suggesting higher uptake rate of these NPs by neurons. The small-size portion of medium-charge NPs yielded weaker and unevenly distributed fluorescence signals in both the blood vessels and the retina tissue. Most of the fluorescence signals were in the big main vessels and the surrounding tissue (Figure 23C & 24C1; Arrows), and signals were undetectable in the small peripheral vessels (Figure 24C1; Arrows). The high-charge NPs accumulated more in the small peripheral vessels and distributed only in the small region along the vessels (Figure 23D & 24D1; Arrows).

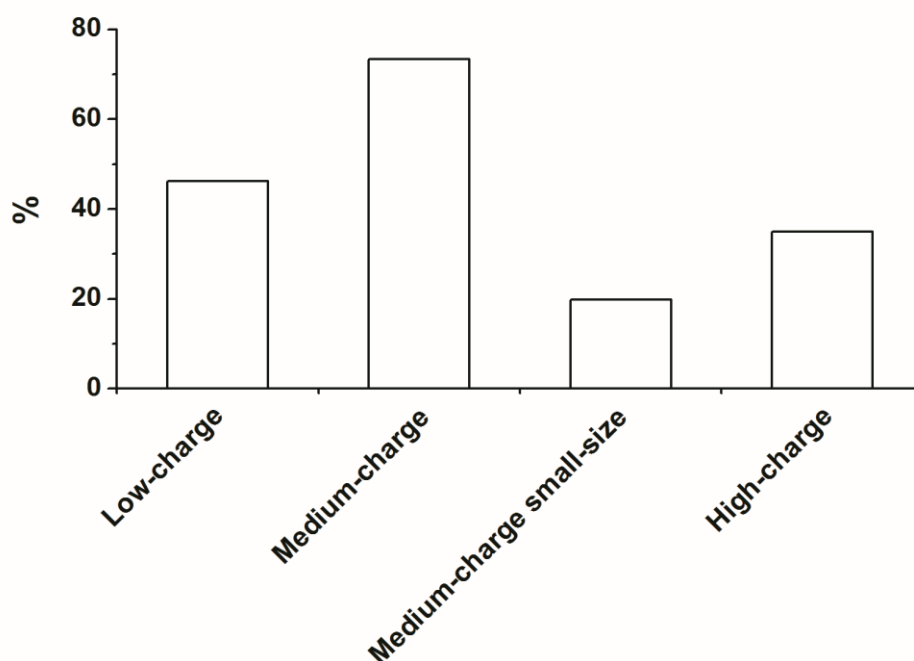


**Figure 22.** Percentage of RGCs with accumulated PDD PBCA NPs over total amount of RGCs.

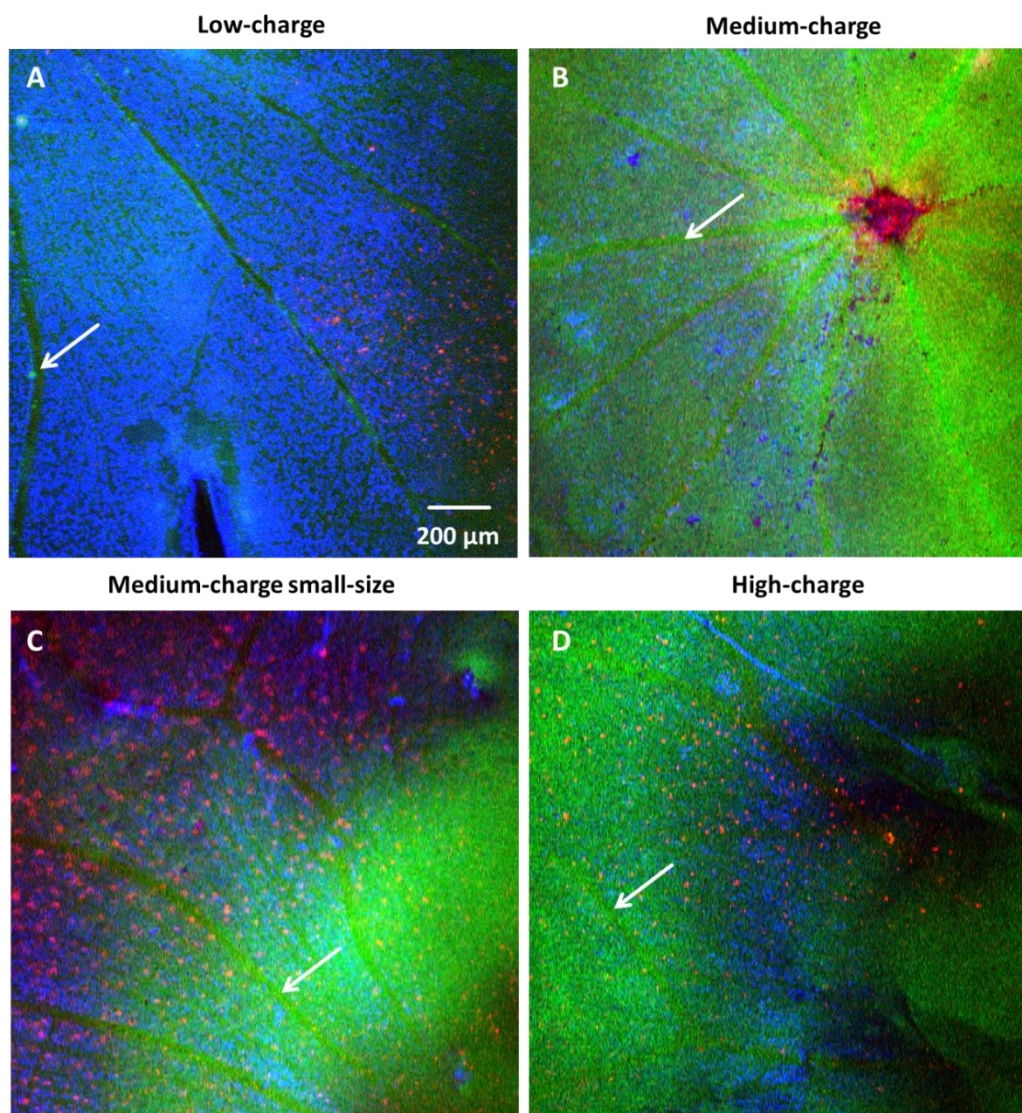


**Figure 23.** Representative *ex vivo* imaging of fluorescence signals in the retina tissue under 5 × magnification 30 min after *i.v.* administration of PDD PBCA NPs. RGCs were retrogradely labeled with carboxylate-modified microspheres in red. Nuclei were stained with Hoechst 33342 in blue. NPs were labeled with Rhodamine 123 in green. (A) Some agglomerates of the low-charge NPs attached on the surface of the vessel walls; (B) The medium-charge NPs yielded stronger and more evenly distributed fluorescence signals in the blood vessels than the low-charge and high-charge NPs; (C) For the small-size portion of medium-charge NPs, most of the fluorescence signals were in the big main vessels and the surrounding tissue; (D) The high-charge NPs accumulated more in the small peripheral vessels and the surrounding tissue.

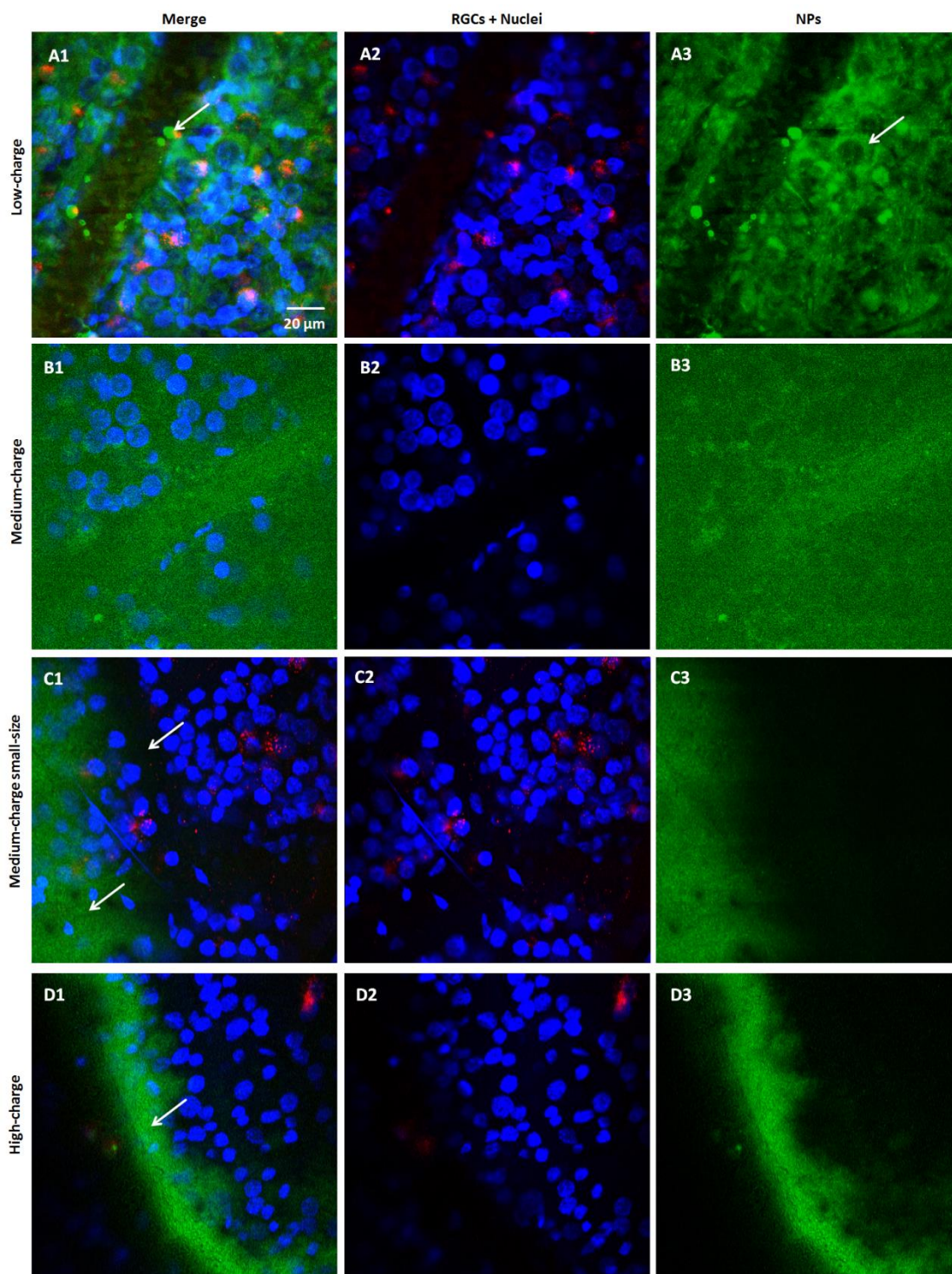


**Figure 24.** Representative *ex vivo* imaging of fluorescence signals in the retina tissue under  $50\times$  magnification 30 min after *i.v.* administration of PDD PBCA NPs. RGCs were retrogradely labeled with carboxylate-modified microspheres in red. Nuclei were stained with Hoechst 33342 in blue. NPs were labeled with Rhodamine 123 in green. (A) The low-charge

NPs accumulated unevenly in the vessel walls and some agglomerates attached on the surface of the vessel walls, and most of the fluorescence signals distributed inside the cells were outside of nuclei; (B) The medium-charge NPs yielded more evenly distributed fluorescence signals in the retina tissue than the low-charge and high-charge NPs; (C) For the small-size portion of medium-charge NPs, most of the fluorescence signals were in the big main vessels and the surrounding tissue, and signals were undetectable in the small peripheral vessels; (D) The high-charge NPs distributed in the small region along the vessels.

### **3.3.3 Biodistribution in the brain and peripheral organs**

To determine whether the physicochemical parameters “surface charge” and “size” affects their biodistribution in the brain and other main organs, I analyzed the accumulation (% dose/g tissue) of four variations of PDD PBCA NPs in the blood, brain, heart, kidney, liver, lung and spleen 30 min after *i.v.* injection of NPs (Figure 25 & 26).

The medium-charge NPs accumulated significantly more in the brain than the low-charge NPs. The higher the surface charge, the more the NPs accumulate in the liver. The small-size portion of medium-charge NPs were cleared from the blood rather quickly and accumulated significantly less in the brain and more in the kidney, liver and spleen than the original NP solution. For all variations of NPs, over half dose accumulated the liver, lung and spleen.

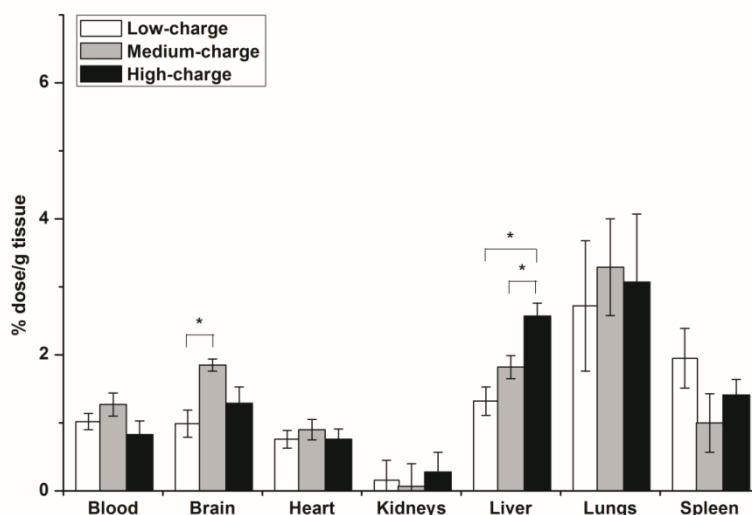


**Figure 25.** Biodistribution of PDD PBCA NPs with different surface charge in brain and other main organs of rats 30 min after *i.v.* administration (n = 5,  $\bar{x} \pm s$ ). \*P < 0.05, compared between groups.

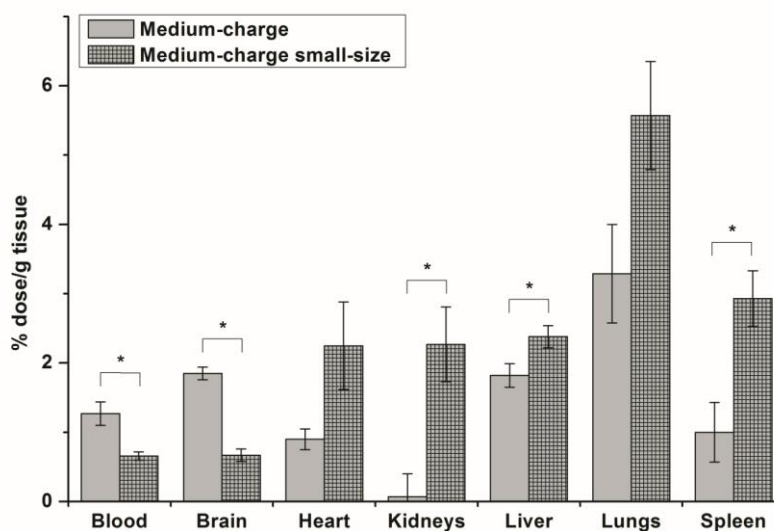


**Figure 26.** Biodistribution of medium-charge PDD PBCA NPs with different size in brain and other main organs of rats 30 min after *i.v.* administration (n = 5,  $\bar{x} \pm s$ ). \*P < 0.05, compared between the small-size portion and the original NP suspension.

### 3.4 Discussion

The central aim of neuropharmacology is to develop drugs to treat diseases of the brain including the retina to achieve neural rescue of regeneration and restoration/repair. However, because most potential drugs can not pass the BBB, BBB-transcytosome NPs may be used as a vehicle to deliver drugs across this barrier, which are then released within the CNS tissue in a therapeutically relevant concentration and time profile. An important goal is that the drug carrier is able to accumulate in an effective concentration mainly in the target organ and avoid a high accumulation in other (peripheral) organs. But the design of an effective and efficient drug carrier that meets all these requirements is quite complex and therefore the NP features that influence a targeted BBB passage and the fate of NPs need to be better understood.

After *i.v.* injection, the PDD PBCA NPs interact first with blood components. The blood contains hundreds of different proteins which contribute to the recognition of foreign materials (Hu Z, *et al.*, 2014; Lai W, *et al.*, 2017; Nguyen VH, *et al.*, 2017; Xiao W, *et al.*, 2018). When NPs come into contact with blood, proteins will immediately adsorb onto the surface and form a so-called protein corona (Cedervall T, *et al.*, 2007). The protein corona changes the size, shape and surface chemistry, and the biological identity of the NPs may have quite different characteristics as compared to their state immediately after production (Lai W, *et al.*, 2017; Nguyen VH, *et al.*, 2017; Xiao W, *et al.*, 2018). Chaudhari KR *et al.* compared aggregation resistance property of PEGylated and non-PEGylated NPs using salt-induced aggregation and serum-induced aggregation techniques and found that PBCA-PEG20 NPs and PBCA-PEG-PBCA NPs displayed exceptionally high resistance to aggregation (Chaudhari KR, *et al.*, 2012). Regarding my PBCA NP variations, my previous results revealed that the low- and high-charge NPs agglomerated after *in vitro* incubation with serum. Especially high-charge NPs agglomerated rather quickly. Using an

approach of *ex vivo* imaging of retina, I now showed that the low-charge NPs accumulated unevenly in vessel walls and agglomerates attached on the surface of the vessel walls (Figure 23A & 24A1; Arrows). In line with these results, I now demonstrated that the high-charge NPs preferentially accumulate in the small peripheral vessels and distribute only in a small region around and along the vessels (Figure 23D & 24D1; Arrows). It seems that NPs with the appropriate surface modification, medium-charge as in my case, have higher aggregation resistance property in the blood to avoid agglomeration and decrease the risk of blood clots.

During blood circulation another challenge is to prevent the PDD PBCA NPs from rapidly degrading and being removed by cells of the mononuclear phagocyte system (MPS). The MPS consists of dendritic cells, blood monocytes, macrophages in liver, spleen and lymph nodes, all of which are responsible for clearing, processing and degrading foreign molecules from the body (Jokerst JV, *et al.*, 2011). It is reported that almost all NPs injected without a stealth strategy (*i.e.*, surface modification) are cleared by the MPS from the blood circulation within a few hours (Moghimi SM, *et al.*, 2001). In mice the clearance of PBCA NPs after intravenous injection occurs already within 5 min (Pardridge WM, 1992). For the PDD PBCA NPs, I observed a clearance of NPs from the retina blood vessels within a time of 30 min, and this clearance rate is influenced by the size and surface properties of NPs. The small-size portion of medium-charge PDD PBCA NPs degraded relatively slowly when incubated with serum *in vitro*, but they were cleared from the blood rather quickly *in vivo* and accumulated significantly less in the brain and more in the kidney, liver and spleen (Figure 26). For all variations of NPs, over half of the dose accumulated in the liver, lung and spleen (Figure 25 and 26). The higher the surface charge, the more did the NPs accumulate in the liver. It is reported that other polymeric NPs with high surface charge were also phagocytized more efficiently by murine macrophages (He C, *et al.*, 2010). Thus, it seems that size and surface properties of NPs can influence their blood circulation time and alter their body distribution. Similarly, Ambruosi *et al.*

(Ambruosi A, *et al.*, 2005) also injected PBCA NPs intravenously in rats and observed the highest NP concentrations in the liver, lung and spleen. Coating the NPs with a negatively-charged Tween 80 decreased the accumulation in these organs and increased the accumulation in the brain, while loading with positive-charged doxorubicin has the opposite effect.

A long circulation time is preferred when designing an effective drug carrier. Up to date, the most promising method to reach this aim are surface chemical modifications by either coating NPs with hydrophilic surfactant or by preparing NPs with covalently-linked Polyethylene glycol (PEG). The antiopsonization strategy of PEGylation has been found to be more effective in preventing phagocytosis than other strategies such as dextran conjugation (Lacava LM, *et al.*, 2001) and dendrimers (Strable E, *et al.*, 2001). By attaching a non-ionic and hydrophilic PEG-layer on the NP surface, the circulation time in the body was significantly increased (Jokerst JV, *et al.*, 2011). However, with a long circulation time there is also the potential risk of accumulation in peripheral, non-target organs, and NPs could end up in places where they are not supposed to be. This increases the risk of unwanted side effects. Moreover, this accumulation in peripheral, non-target organs can lead to a “steal effect”, *i.e.*, because of the clearance in other organs the number of NPs available for accumulation in the brain is markedly lowered. My results concerning the biodistribution of PDD PBCA NPs support this hypothesis. My PDD PBCA NPs are aimed at targeting the brain. In general, a higher blood concentration leads to a higher brain concentration (Figure 25 and 26), which means a longer circulation time facilitates brain delivery. However, my data indicate that not only the surface characteristics but also the size influence the circulation time: the higher up-take of small-size NPs in peripheral organs significantly decreased their accumulation in the brain as compared to the NP fraction with larger NPs. Using *in vivo* kinetic experiments, the small-size fraction of the medium-charge NPs revealed the lowest signal in the vessels, which was already detected at the moment of the injection.



Moreover, the fluorescent signal of this NP group disappeared fastest. I proposed that after intravenous injection, reaching the heart and being pumped to the lung tissue, the NPs are subject to a kind of “first pass” effect where the small-sized NPs – not the larger ones - can “leak” through the fenestrated vessel walls of the lung’s veins and arteries. Therefore, it seems that size can influence NPs’ kinetic from the very beginning after entering into the blood system. The different up-take rates of peripheral organs has also impacts the cellular distribution of NPs. Co-localization analysis of NPs with RGCs indicates that in general the NPs were internalized by these cells (Figure 24). However, a higher percentage of RCGs were co-localized with the medium-charge NPs as compared to the other NP variations (Figure 22), suggesting a higher uptake of these NPs by neurons. This is a beneficial feature for targeting neurons for protection and restoration.

To summarize my findings: Drug delivery using NPs is a complicated process because after entering the blood circulation following injection, drug carriers have to travel a long way to reach the final target with high efficiency and without unwanted side effects such as high accumulation in other organs of the body with associated risk of causing toxic reactions in the non-target tissue. As I demonstrated, the situation is even more complex because minor changes in the production protocol for NP--carriers can alter physicochemical parameters such as size or zeta-potential, which have great impact on NPs’ interaction with blood components. As a consequence, these conditions significantly alter up-take and interaction with peripheral organs, barriers and neurons. Thus, a better understanding of such parameters can enable scientists to design and use such modifications to develop tailor-made nano-carriers as a means to deliver drugs for the treatment of brain and retina disorders. Because these conditions are very much dependent on the drug (or imaging marker) to be used, there is no “standard” NP composition (“golden bullet”) for drug delivery to modulate the function of the retina or brain to achieve neuroprotection or restoration and repair.

## 4 General discussion

### 4.1 Design of the Studies

In order to study NPs' passage across the BRB in living animals – a suitable surrogate model of the BBB – I carried out real-time *in vivo* imaging of blood vessels and retina tissue before and several time points after intravenous injection (Sabel BA, *et al.*, 1997; Rousseau V, *et al.*, 1999 and 2001; Prilloff S, *et al.*, 2007 and 2010; Henrich-Noack P, *et al.*, 2012; Voigt N, *et al.*, 2014; Khalid MK, *et al.*, 2018). Whereas in the previous work on BRB passage of nanosystems we studied the influence of different surfactants (Voigt N, *et al.*, 2014), I now have advanced the analysis to obtain semi-quantitative data on the kinetic profiles of fluorescence-labeled NPs and compared the NPs' BRB passage efficiency by determining the fluorescence signals in blood vessels and retina tissue.

Our earlier tests of different surfactants for NP production indicated that basically negatively as well as positively-charged PBCA NPs can cross the BRB and also larger size was not a hindrance as NPs with Z-average size of 130 nm and 422 nm yielded fluorescent signals in the tissue (Voigt N, *et al.*, 2014). However, for possible future applications as drug carriers, the most efficient nanoparticulate system needs to be identified. I therefore focused on optimizing the PDD PBCA NPs. This kind of NP was selected as it comprises the most promising variant from prior studies and pilot experiments.

In agreement with earlier observations I found the modification of the surface-coating-complex has a considerable influence on BRB passage of NPs: when altering the surface of the PDD NPs by adsorption of Rhodamine 123, the uptake into retina tissue was clearly lower than that of NPs with DEAE-dextran surfactant coating only where the Rhodamine 123 was incorporated (Figure 13). I therefore continued my experiments with the NPs which contained the incorporated Rhodamine 123 tracer

and which was coated only with DEAE-dextran.

## **4.2 Protein corona-first interaction with blood**

After *i.v.* injection, the PDD PBCA NPs interact first with blood components. The blood contains hundreds of different proteins which contribute to the recognition of foreign materials (Hu Z, *et al.*, 2014; Lai W, *et al.*, 2017; Nguyen VH, *et al.*, 2017; Xiao W, *et al.*, 2018). When NPs come into contact with blood, proteins will immediately adsorb onto the surface and form a so-called protein corona (Cedervall T, *et al.*, 2007). The protein corona changes the size, shape and surface chemistry, and the biological identity of the NPs may have quite different characteristics as compared to their state immediately after production (Lai W, *et al.*, 2017; Nguyen VH, *et al.*, 2017; Xiao W, *et al.*, 2018).

## **4.3 Degradation and agglomeration in blood**

Chaudhari KR *et al.* (2012) compared aggregation resistance property of PEGylated and non-PEGylated NPs using salt-induced aggregation and serum-induced aggregation techniques and found that PBCA-PEG20 NPs and PBCA-PEG-PBCA NPs displayed exceptionally high resistance to aggregation. Regarding my PBCA NP variations, the results revealed that the low- and high-charge NPs agglomerated after *in vitro* incubation with serum. Especially high-charge NPs agglomerated rather quickly. Now through *ex vivo* imaging of retina, I showed that the low-charge NPs accumulated unevenly in vessel walls and confirmed agglomerates attached on the surface of the vessel walls (Figure 23A & 24A1; Arrows). Also in line with these results, I now demonstrated that the high-charge NPs preferentially accumulate in the small peripheral vessels and distribute only in a small region along the vessels (Figure

23D & 24D1; Arrows). It seems that NPs with the appropriate surface modification, medium-charge as in my case, have higher aggregation resistance property in the blood to avoid agglomeration and decrease the risk of blood clots. Surface charge and size considerably also influenced the degradation speed of the NPs in the blood. A small portion of the low-charge NPs was found to be decreased in size after 10 min of serum incubation (Figure 10A), probably indicating degradation. The SEM images indicate that the high-charge NPs virtually disappeared after 10 min incubation in serum (Figure 11D2). One possible explanation is that this positive charge facilitates an interaction with negatively-charged serum-components like albumins which may facilitate solubilization. Stein and Hamacher also carried out degradation tests on PBCA NPs in dog serum, and almost complete hydrolysis was observed within 3.5 h (Stein M, *et al.*, 1992).

#### **4.4 Clearance by the MPS**

During blood circulation another challenge is to prevent the PDD PBCA NPs from rapidly degrading and being removed by cells of the mononuclear phagocyte system (MPS). The MPS consists of dendritic cells, blood monocytes, macrophages in liver, spleen and lymph nodes, all of which are responsible for clearing, processing and degrading foreign objects from the body (Jokerst JV, *et al.*, 2011). It is reported that almost all NPs injected without a stealth strategy (*i.e.*, surface modification) are cleared by the MPS from the blood circulation within a few hours (Moghimi SM, *et al.*, 2001). In mice the clearance of PBCA NPs after intravenous injection occurs already within 5 min (Pardridge WM, 1992). For the PDD PBCA NPs, I observed a clearance of NPs from the retina blood vessels within a time of 30 min, and this clearance rate is influenced by the size and surface properties of NPs (Figure 15 & 16). The small-size portion of medium-charge PDD PBCA NPs degraded relatively slowly when incubated with serum *in vitro* (Table 3 and Figure 10 & 11), but they were

cleared from the blood rather quickly *in vivo* and accumulated significantly less in the brain and more in the kidney, liver and spleen (Figure 26). For all variations of NPs, over half of the dose accumulated in the liver, lung and spleen (Figure 25 & 26). The higher the surface charge, the more did the NPs accumulate in the liver. Thus, it seems that size and surface properties of NPs can influence their blood circulation time and alter their body distribution. Similarly, Ambruosi *et al.* (2005) also injected PBCA NPs intravenously in rats and observed the highest NP concentrations in the liver, lung and spleen. Coating the NPs with a negatively-charged Tween 80 decreased the accumulation in these organs and increased the accumulation in the brain, while loading with positively-charged doxorubicin has the opposite effect.

#### **4.5 Effects on circulation time**

A long circulation time is preferred when designing an effective drug carrier. Up to date, the most promising method to reach this aim are surface chemical modifications by either coating NPs with hydrophilic surfactant or by preparing NPs with covalently-linked Polyethylene glycol (PEG). As an antiopsonization strategy, PEGylation has been proven more effective to prevent phagocytosis than other strategies such as dextran conjugation (Lacava LM, *et al.*, 2001) and dendrimers (Strable E, *et al.*, 2001). By attaching a non-ionic and hydrophilic PEG-layer on the NP surface, the circulation time in the body was significantly increased (Jokerst JV, *et al.*, 2011). However, with a long circulation time there is also the potential risk of accumulation in peripheral, non-target organs, and NPs could end up in places where they are not supposed to be, which increases the risk of unwanted side effects. Moreover, this accumulation in peripheral, non-target organs can lead to a “steal effect”, *i.e.*, because of the clearance in other organs the NPs available for accumulation in the brain is lowered. My results concerning the biodistribution of PDD PBCA NPs support this hypothesis. My PDD PBCA NPs are aimed at targeting

the brain. In general, a higher blood concentration leads to a higher brain concentration (Figure 25 & 26), which means a longer circulation time facilitates the brain delivery. However, my data indicate that not only the surface characteristics influence the circulation time but also the size: the higher up-take of small-size NPs in peripheral organs significantly decreased their accumulation in the brain as compared to the NP fraction with larger NPs. This has also consequences for the cellular distribution of NPs. Co-localization analysis of NPs with RGCs indicates that in general the NPs were internalized by these cells (Figure 24). However, a higher percentage of RCGs were co-localized with the medium-charge NPs as compared to the other NP variations (Figure 22), suggesting a higher uptake of these NPs by neurons. This is a beneficial feature for targeting neurons for protection and restoration.

#### **4.6 Possible mechanisms of passage**

So far, research projects on BRB passage of NPs have indicated that surfactants are a key factor for successful brain delivery. Among the surfactants investigated, Tween 80 has long been considered to represent a “gold standard” for effective brain delivery of PBCA NPs (Kreuter J, *et al.*, 2003). In the current work I used nonionic poloxamer 188 as surfactant. Both Tween 80 and poloxamer 188, being rather different in their chemical structures, still show very similar plasma protein adsorption patterns on PBCA NPs loaded with doxorubicin, with a remarkably high amount of apolipoprotein A, the major apolipoprotein component of high density lipoproteins (Petri B, *et al.*, 2007). It is known that the poloxamers - block-copolymers of poly (propylene oxide) and poly (ethylene oxide) – interact with cell membranes and, in particular, with lecithin, their essential component (Zhirnov AE, *et al.*, 2005). It was suggested that the preferred brain uptake of nanoparticulate systems with such surfactants are due to an affinity to lecithin and apolipoproteins (Kreuter J, *et al.*,

2007). Therefore it is possible that coating with poloxamer 188 can assist these kinds of receptor-mediated uptake. However, my PDD NPs appeared in the retina tissue 5 min after injection and the peak concentration was achieved 30 min after injection (Figure 11). The passage through the BRB was too fast to consider only receptor-mediated uptake. Gulyaev *et al.* showed that the peak concentration of the doxorubicin loaded in the Tween 80-coated PBCA NPs in the rat brain was achieved 2 h after intravenous injection (Gulyaev AE, *et al.*, 1999), which is the typical time course for receptor-mediated uptake. In addition, I used cationic DEAE-dextran as stabilizer. As a widely-used transfection reagent, it binds negatively-charged DNA to form a complex which can be taken up by cells via adsorptive endocytosis (Smale ST, *et al.*, 2010). Therefore I assume that endocytosis may be the mechanism for the passage of my PDD PBCA NPs across the negatively-charged BRB. In this respect, also the size may affect the endocytotic uptake mechanism. Generally, clathrin-mediated endocytosis was suggested to be the predominant pathway for the uptake of small particles below 200 nm, whereas the uptake of larger particles up to a size of 500 nm seems to be caveolae-mediated (Hillaireau H, *et al.*, 2009).

## 4.7 General conclusions

After entering the blood circulation following injection, it is a long distance for a drug carrier to reach the final target with high efficiency and without high accumulation in other organs of the body with the associated risk of causing toxic side effects. To summarize my findings: minor changes in the production protocol for nano-carriers can alter physicochemical parameters such as size or surface charge, which probably have great impact on NPs' interaction with blood components. As a consequence, these conditions significantly alter up-take and interaction with peripheral organs, barriers and neurons. A better understanding of these factors can thus enable scientists to design and use such modifications to develop tailor-made nano-carriers as a means

to deliver drugs for the treatment of brain and retina disorders. Apparently, there are no standard rules for the design of nanoparticulate carriers for brain delivery; each nano-system requires its own design and optimization. In case of PDD PBCA NP, larger size and a medium zeta-potential were found to be the preferred variant to achieve BRB passage. However, the application of these carriers is abroad, not only for single chemical drugs, but also for multiple extracts. For example, Wang J, *et al.* performed cell experiments on Lycium barbarum polysaccharide which was encapsulated into electrospun nanofibers and found it could be a potential candidate as tissue engineered scaffold for peripheral nerve regeneration (Wang J, *et al.*, 2018). Anyway, more research is worthwhile for further exploring the feasibility and versatility of NPs as possible vehicles for drug delivery.



## 5 References

Alyautdin RN, Petrov VE, Langer K, Berthold A, Kharkevich DA & Kreuter J. (1997). Delivery of loperamide across the blood-brain barrier with polysorbate 80-coated polybutylcyanoacrylate nanoparticles. *Pharm Res.* 14, 325-328.

Alyautdin RN, Tezиков EB, Ränge P, Kharkevich DA, Begley DJ & Kreuter J. (1998). Significant entry of tubocurarine into the brain of rats by adsorption to polysorbate 80-coated polybutylcyanoacrylate nanoparticles: an in situ brain perfusion study. *J Microencapsul.* 15, 67-74.

Ambruosi A, Yamamoto H & Kreuter J. (2005). Body distribution of polysorbate-80 and doxorubicin-loaded [14C]poly(butyl cyanoacrylate) nanoparticles after i.v. administration in rats. *J Drug Target.* 13, 535-542.

Begley DJ. (1996). The blood-brain barrier: principles for targeting peptides and drugs to the central nervous system. *J Pharm Pharmacol.* 48, 136-146.

Béduneau A, Saulnier P & Benoit JP. (2007). Active targeting of brain tumors using nanocarriers. *Biomaterials.* 28, 4947-4967.

Bhunia SK, Saha A, Maity AR, Ray SC & Jana NR. (2013). Carbon nanoparticle-based fluorescent bioimaging probes. *Sci Rep.* 3, 1473.

Brigger I, Morizet J, Aubert G, Chacun H, Terrier-Lacombe MJ, Couvreur P & Vassal G. (2002). Poly(ethylene glycol)-coated hexadecylcyanoacrylate nanospheres display a combined effect for brain tumor targeting. *J Pharmacol Exp Ther.* 303, 928-936.

Campbell M, Humphries P. (2011). Size-selective and in vitro assessment of inner blood retina barrier permeability. *Methods Mol Biol.* 763, 355-367.

Cedervall T, Lynch I, Lindman S, Berggård T, Thulin E, Nilsson H, Dawson KA & Linse S. (2007). Understanding the nanoparticle-protein corona using methods to

quantify exchange rates and affinities of proteins for nanoparticles. *Proc Natl Acad Sci U S A*. 104, 2050-2055.

Chaudhari KR, Ukawala M, Manjappa AS, Kumar A, Mundada PK, Mishra AK, Mathur R, Mönkkönen J & Murthy RS. (2012). Opsonization, biodistribution, cellular uptake and apoptosis study of PEGylated PBCA nanoparticle as potential drug delivery carrier. *Pharm Res*. 29, 53-68.

Cordon-Cardo C, O'Brien JP, Casals D, Rittman-Grauer L, Biedler JL, Melamed MR & Bertino JR. (1989). *Proc Natl Acad Sci U S A*. 86, 695-698.

Cunha-Vaz J, Bernardes R & Lobo C. (2011). Blood-retinal barrier. *Eur J Ophthalmol*. 21 Suppl 6, S3-9.

Dagenais C, Rousselle C, Pollack GM & Scherrmann JM. (2000). Development of an in situ mouse brain perfusion model and its application to mdrla P-glycoprotein-deficient mice. *J Cereb Blood Flow Metab*. 20, 381-386.

Elmquist WF & Sawchuk RJ. (1997). Application of microdialysis in pharmacokinetic studies. *Pharm Res*. 14, 267-288.

Freese C, Hanada S, Fallier-Becker P, Kirkpatrick CJ & Unger RE. (2017). Identification of neuronal and angiogenic growth factors in an in vitro blood-brain barrier model system: Relevance in barrier integrity and tight junction formation and complexity. *Microvasc Res*. 111, 1-11.

Frenkel V. (2008). Ultrasound mediated delivery of drugs and genes to solid tumors. *Adv Drug Deliv Rev*. 60, 1193-1208.

Gabathuler R. (2010). Approaches to transport therapeutic drugs across the blood-brain barrier to treat brain diseases. *Neurobiol Dis*. 37, 48-57.

Galla HJ. (2018). Monoculture of primary porcine brain capillary endothelial cells:

Still a functional in vitro model for the blood-brain-barrier. *J Control Release*. 285, 172-177.

Gao K & Jiang X. (2006). Influence of particle size on transport of methotrexate across blood brain barrier by polysorbate 80-coated polybutylcyanoacrylate nanoparticles. *Int J Pharm*. 310, 213-219.

Gelperina SE, Khalansky AS, Skidan IN, Smirnova ZS, Bobruskin AI, Severin SE, Turowski B, Zanella FE & Kreuter J. (2002). Toxicological studies of doxorubicin bound to polysorbate 80-coated poly(butyl cyanoacrylate) nanoparticles in healthy rats and rats with intracranial glioblastoma. *Toxicol Lett*. 126, 131-141.

Goldmann EE. (1912). Neue Untersuchungen über die äussere und innere Sekretion des gesunden und kranken Organismus im Lichte der "vitalen Färbung". *Dtsch. Z. Nervenheilkd*. 117, 403-404.

Grabrucker AM, Ruozi B, Belletti D, Pederzoli F, Forni F, Vandelli MA & Tosi G2. (2016). Nanoparticle transport across the blood brain barrier. *Tissue Barriers*. 25, 4(1):e1153568.

Gulyaev AE, Gelperina SE, Skidan IN, Antropov AS, Kivman GY & Kreuter J. (1999). Significant transport of doxorubicin into the brain with polysorbate 80-coated nanoparticles. *Pharm Res*. 16, 1564-1569.

Hans ML & Lowman AM. (2002). Biodegradable nanoparticles for drug delivery and targeting. *Curr Opin Solid State Mater Sci*. 6, 319-327.

Hansali F, Poisson G, Wu M, Bendedouch D & Marie E. (2011). Miniemulsion polymerizations of n-butyl cyanoacrylate via two routes: towards a control of particle degradation. *Colloids Surf B Biointerfaces*. 88, 332-338.

- He C, Hu Y, Yin L, Tang C & Yin C. (2010). Effects of particle size and surface charge on cellular uptake and biodistribution of polymeric nanoparticles. *Biomaterials*. 31, 3657-3666.
- Henrich-Noack P, Prilloff S, Voigt N, Jin J, Hintz W, Tomas J & Sabel BA. (2012). In vivo visualisation of nanoparticle entry into central nervous system tissue. *Arch Toxicol*. 86, 1099-1105.
- Hernot S & Klibanov AL. (2008). Microbubbles in ultrasound-triggered drug and gene delivery. *Adv Drug Deliv Rev*. 60, 1153-1166.
- Hervé F, Ghinea N, Scherrmann JM. (2008). CNS delivery via adsorptive transcytosis. *AAPS J*. 10, 455-472.
- Hillaireau H & Couvreur P. (2009). Nanocarriers' entry into the cell: relevance to drug delivery. *Cell Mol Life Sci*. 66, 2873-2896.
- Hu Z, Zhang H, Zhang Y, Wu R & Zou H. (2014). Nanoparticle size matters in the formation of plasma protein coronas on Fe<sub>3</sub>O<sub>4</sub> nanoparticles. *Colloids Surf B Biointerfaces*. 121, 354-361.
- Jokerst JV, Lobovkina T, Zare RN & Gambhir SS. (2011). Nanoparticle PEGylation for imaging and therapy. *Nanomedicine (Lond)*. 6, 715-728.
- Jones AR & Shusta EV. (2007). Blood-brain barrier transport of therapeutics via receptor-mediation. *Pharm Res*. 24, 1759-1771.
- Jouan E, Le Vée M, Mayati A, Denizot C, Parmentier Y & Fardel O. (2016). Evaluation of P-glycoprotein inhibitory potential using a rhodamine 123 accumulation assay. *Pharmaceutics*. 8, pii:E12.
- Kreuter J, Alyautdin RN, Kharkevich DA & Ivanov AA. (1995). Passage of peptides through the blood-brain barrier with colloidal polymer particles (nanoparticles). *Brain*

*Res.* 674, 171-174.

Kreuter J, Hekmatara T, Dreis S, Vogel T, Gelperina S & Langer K. (2007). Covalent attachment of apolipoprotein A-I and apolipoprotein B-100 to albumin nanoparticles enables drug transport into the brain. *J Control Release.* 118, 54-58.

Kreuter J, Ränge P, Petrov V, Hamm S, Gelperina SE, Engelhardt B, Alyautdin R, von Briesen H & Begley DJ. (2003). Direct evidence that polysorbate-80-coated poly (butylcyanoacrylate) nanoparticles deliver drugs to the CNS via specific mechanisms requiring prior binding of drug to the nanoparticles. *Pharm Res.* 20, 409-416.

Khalid MK, Asad M, Henrich-Noack P, Sokolov M, Hintz W, Grigartzik L, Zhang E, Dityatev A, van Wachem B & Sabel BA. (2018). Evaluation of Toxicity and Neural Uptake In Vitro and In Vivo of Superparamagnetic Iron Oxide Nanoparticles. *Int J Mol Sci.* 19, pii: E2613.

Lacava LM, Lacava ZG, Da Silva MF, Silva O, Chaves SB, Azevedo RB, Pelegrini F, Gansau C, Buske N, Sabolovic D & Morais PC. (2001). Magnetic resonance of a dextran-coated magnetic fluid intravenously administered in mice. *Biophys J.* 80, 2483-2486.

Lai W, Wang Q, Li L, Hu Z, Chen J & Fang Q. (2017). Interaction of gold and silver nanoparticles with human plasma: Analysis of protein corona reveals specific binding patterns. *Colloids Surf B Biointerfaces.* 152, 317-325.

Luissint AC, Artus C, Glacial F, Ganeshamoorthy K & Couraud PO. (2012). Tight junctions at the blood brain barrier: physiological architecture and disease-associated dysregulation. *Fluids Barriers CNS.* 9, 23.

Maeda H, Wu J, Sawa T, Matsumura Y & Hori K. (2000). Tumor vascular permeability and the EPR effect in macromolecular therapeutics: a review. *J Control Release.* 65, 271-284.

- Mailander V & Landfester K. (2009). Interaction of nanoparticles with cells. *Biomacromolecules*. 10, 2379-2400.
- Mayer F, Mayer N, Chinn L, Pinsonneault RL, Kroetz D & Bainton RJ. (2009) Evolutionary conservation of vertebrate blood-brain barrier chemoprotective mechanisms in *Drosophila*. *J Neurosci*. 29, 3538-3550.
- Moghimi SM, Hunter AC & Murray JC. (2001). Long-circulating and target specific nanoparticles: theory to practice. *Pharmacol Rev*. 53, 283-318.
- Mosqueira VCF, Legrand P, Gref R, Heurtault B, Appel M & Barratt G. (1999). Interactions between a macrophage cell line (J774A1) and surface-modified poly (D, L-lactide) nanocapsules bearing poly(ethylene glycol). *J Drug Targeting*. 7, 65-78.
- Nguyen VH & Lee BJ. (2017). Protein corona: a new approach for nanomedicine design. *Int J Nanomedicine*. 12, 3137-3151.
- Olivier JC, Fenart L, Chauvet R, Pariat C, Cecchelli R & Couet W. (1999). Indirect evidence that drug brain targeting using polysorbate 80-coated polybutylcyanoacrylate nanoparticles is related to toxicity. *Pharm Res*. 16, 1836-1842.
- Pauletti GM, Okumu FW & Borchardt RT. (1997). Effect of size and charge on the passive diffusion of peptides across Caco-2 cell monolayers via the paracellular pathway. *Pharm Res*. 14, 164-168.
- Pardridge WM. (1992). Recent developments in peptide drug delivery to the brain. *Pharmacol Toxicol*. 71, 3-10.
- Pardridge WM. (1998). CNS drug design based on principles of blood-brain barrier transport. *J Neurochem*. 70, 1781-1792.
- Pardridge WM. (2005). The blood-brain barrier: bottleneck in brain drug development. *NeuroRx*. 2, 3-14.

- Pardridge WM. (2007). Drug targeting to the brain. *Pharm Res.* 24, 1733-1744.
- Pereverzeva E, Treschalin I, Bodyagin D, Maksimenko O, Langer K, Dreis S, Asmussen B, Kreuter J & Gelperina S. (2007). Influence of the formulation on the tolerance profile of nanoparticle-bound doxorubicin in healthy rats: focus on cardio- and testicular toxicity. *Int J Pharm.* 337, 346-356.
- Pereverzeva E, Treschalin I, Bodyagin D, Maksimenko O, Kreuter J & Gelperina S. (2008). Intravenous tolerance of a nanoparticlebased formulation of doxorubicin in healthy rats. *Toxicol Lett.* 178, 9-19.
- Petri B, Bootz A, Khalansky A, Hekmatara T, Müller R, Uhl R, Kreuter J & Gelperina S. (2007). Chemotherapy of brain tumour using doxorubicin bound to surfactant-coated poly(butyl cyanoacrylate) nanoparticles: revisiting the role of surfactants. *J Control Release.* 117, 51-58.
- Prilloff S, Fan J, Henrich-Noack P & Sabel BA. (2010). In vivo confocal neuroimaging (ICON): non-invasive, functional imaging of the mammalian CNS with cellular resolution. *Eur J Neurosci.* 31, 521-528.
- Prilloff S, Noblejas MI, Chedhomme V & Sabel BA. (2007). Two faces of calcium activation after optic nerve trauma: life or death of retinal ganglion cells in vivo depends on calcium dynamics. *Eur J Neurosci.* 25, 3339-3346.
- Pulicherla KK & Verma MK. (2015). Targeting therapeutics across the blood brain barrier (BBB), prerequisite towards thrombolytic therapy for cerebrovascular disorders-an overview and advancements. *AAPS PharmSciTech.* 16, 223-233.
- Ränge P, Unger RE, Oltrogge JB, Zenker D, Begley D, Kreuter J & Von Briesen H. (2000). Polysorbate-80 coating enhances uptake of polybutylcyanoacrylate (PBCA)-nanoparticles by human and bovine primary brain capillary endothelial cells. *Eur J Neurosci.* 12, 1931-1940.

Rempe R, Cramer S, Hüwel S & Galla HJ. (2011). Transport of Poly(n-butylcyano-acrylate) nanoparticles across the blood-brain barrier in vitro and their influence on barrier integrity. *Biochem Biophys Res Commun.* 406, 64-69.

Reichel A. (2006). The role of blood-brain barrier studies in the pharmaceutical industry. *Curr Drug Metab.* 7, 183-203.

Rousseau V & Sabel BA. (2001). Restoration of vision IV: role of compensatory soma swelling of surviving retinal ganglion cells in recovery of vision after optic nerve crush. *Restor Neurol Neurosci.* 18, 177-189.

Rousseau V, Engelmann R & Sabel BA. (1999). Restoration of vision III: soma swelling dynamics predicts neuronal death or survival after optic nerve crush in vivo. *Neuroreport.* 10, 3387-3391.

Ribatti D, Nico B, Crivellato E & Artico M. (2006). Development of the blood-brain barrier: a historical point of view. *Anat Rec B New Anat.* 289, 3-8.

Sabel BA, Engelmann R & Humphrey MF. (1997). In vivo confocal neuroimaging (ICON) of CNS neurons. *Nat Med.* 3, 244-247.

Smale ST. (2010). DEAE-dextran transfection of lymphocyte cell lines. *Cold Spring Harb Protoc.* 2010, pdb.prot5373.

Stein M & Hamacher E. (1992). Degradation of polybutyl 2-cyanoacrylate microparticles, *Int J Pharm.* 80, R11-13.

Steuer H, Jaworski A, Elger B, Kaussmann M, Keldenich J, Schneider H, Stoll D & Schlosshauer B. (2005). Functional characterization and comparison of the outer blood-retina barrier and the blood-brain barrier. *Invest Ophthalmol Vis Sci.* 46, 1047-1053.

Steuer H, Jaworski A, Stoll D & Schlosshauer B. (2004). In vitro model of the outer



blood-retina barrier. *Brain Res Brain Res Protoc.* 13, 26-36.

Strable E, Bulte JWM, Moskowitz B, Vivekanandan K, Allen M & Douglas T. (2001). Synthesis and characterization of soluble iron oxide-dendrimer composites. *Chem Mater.* 13, 2201-2209.

Thiele L, Diederichs JE, Reszka R, Merkle HP & Walter E. (2003). Competitive adsorption of serum proteins at microparticles affects phagocytosis by dendritic cells. *Biomaterials.* 24, 1409-1418.

Thorne RG & Nicholson C. (2006). In vivo diffusion analysis with quantum dots and dextrans predicts the width of brain extracellular space. *Proc Natl Acad Sci U S A.* 103, 5567-5572.

Tiwari SB & Amiji MM. (2006). A review of nanocarrier-based CNS delivery systems, *Curr Drug Deliv.* 3, 219-232.

Toda R, Kawazu K, Oyabu M, Miyazaki T & Kiuchi Y. (2011). Comparison of drug permeabilities across the blood-retinal barrier, blood-aqueous humor barrier, and blood-brain barrier. *J Pharm Sci.* 100, 3904-3911.

Voigt N, Henrich-Noack P, Kockentiedt S, Hintz W, Tomas J & Sabel BA. (2014). Surfactants, not size or zeta-potential influence blood-brain barrier passage of polymeric nanoparticles. *Eur J Pharm Biopharm.* 87, 19-29.

Voigt N, Henrich-Noack P, Kockentiedt S, Hintz W, Tomas J & Sabel BA. (2014). Toxicity of polymeric nanoparticles in vivo and in vitro. *J Nanopart Res.* 16, pii: 2379.

Wang CX, Huang LS, Hou LB, Jiang L, Yan ZT, Wang YL & Chen ZL. Antitumor effects of polysorbate-80 coated gemcitabine polybutylcyanoacrylate nanoparticles in vitro and its pharmacodynamics in vivo on C6 glioma cells of a brain tumor model. *Brain Res.* 1261, 91-99.

Wang J, Tian L, He L, Chen N, Ramakrishna S, So KF & Mo X. (2018). Lycium barbarum polysaccharide encapsulated Poly lactic-co-glycolic acid Nanofibers: cost effective herbal medicine for potential application in peripheral nerve tissue engineering. *Sci Rep.* 8, 8669.

Wohlfart S, Gelperina S & Kreuter J. (2012). Transport of drugs across the blood-brain barrier by nanoparticles. *J Control Release.* 161, 264-273.

Wu D & Pardridge WM. (1998). Pharmacokinetics and blood-brain barrier transport of an anti-transferrin receptor monoclonal antibody (OX26) in rats after chronic treatment with the antibody. *Drug Metab Dispos.* 26, 937-939.

Xiao W & Gao H. (2018). The impact of protein corona on the behavior and targeting capability of nanoparticle-based delivery system. *Int J Pharm.* 552, 328-339.

Xu N, Gu J, Zhu Y, Wen H, Ren Q & Chen J. (2011). Efficacy of intravenous amphotericin B-polybutylcyanoacrylate nanoparticles against cryptococcal meningitis in mice. *Int J Nanomedicine.* 6, 905-913.

You Q, Hopf T, Hintz W, Rannabauer S, Voigt N, van Wachem B, Henrich-Noack P & Sabel BA. (2018). Major effects on blood-retina barrier passage by minor alterations in design of polybutylcyanoacrylate nanoparticles. *J Drug Target.* 1-25.

Zhirnov AE, Demina TV, Krylova OO, Grozdova ID, Melik-Nubarov NS. (2005). Lipid composition determines interaction of liposome membranes with Pluronic L61. *Biochim Biophys Acta.* 2005; 1720, 73-83.

Zhou Q, Sun X, Zeng L, Liu J & Zhang Z. (2009). A randomized multicenter phase II clinical trial of mitoxantrone-loaded nanoparticles in the treatment of 108 patients with unresected hepatocellular carcinoma. *Nanomedicine.* 5, 419-423.

Zhou Y, Peng Z, Seven ES & Leblanc RM. (2018). Crossing the blood-brain barrier with nanoparticles. *J Control Release.* 270, 290-300.

## **EHRENERKLÄRUNG**

Ich versichere hiermit, dass ich die vorliegende Arbeit ohne unzulässige Hilfe Dritter und ohne Benutzung anderer als der angegebenen Hilfsmittel angefertigt habe; verwendete fremde und eigene Quellen sind als solche kenntlich gemacht.

Ich habe insbesondere nicht wissentlich:

- Ergebnisse erfunden oder widersprüchlich Ergebnisse verschwiegen,
- statistische Verfahren absichtlich missbraucht, um Daten in ungerechtfertigter Weise zu interpretieren,
- fremde Ergebnisse oder Veröffentlichungen plagiiert,
- fremde Forschungsergebnisse verzerrt wiedergegeben.

Mir ist bekannt, dass Verstöße gegen das Urheberrecht Unterlassungs- und Schadensersatz- ansprüche des Urhebers sowie eine strafrechtliche Ahndung durch die Strafverfolgungsbehörden begründen kann.

Ich erkläre mich damit einverstanden, dass die Arbeit ggf. mit Mitteln der elektronischen Datenverarbeitung auf Plagiate überprüft werden kann.

Die Arbeit wurde bisher weder im Inland noch im Ausland in gleicher oder ähnlicher Form als Dissertation eingereicht und ist als Ganzes auch noch nicht veröffentlicht.

Ort, Datum

Unterschrift